J. Fluid Mech. (1987), *vol.* 182, *pp.* 369–409
Printed in Great Britain

Turbulent oscillatory flow over rough beds

By J. F. A. SLEATH
Department of Engineering, University of Cambridge, Trumpington Street, Cambridge CB2 1PZ, UK

(Received 6 August 1986)

Velocity measurements are presented for turbulent oscillatory flow over rough beds. Two components of velocity were measured with a laser-Doppler anemometer and the rough beds consisted of a single layer of sand, gravel or pebbles on a flat surface. Turbulence intensities showed significant variation during the course of the cycle. Maximum turbulence intensity propagated out from the bed at a more or less constant velocity for all beds. Variation of time-mean turbulence intensity with height was qualitatively similar to that observed in steady flows. Reynolds stress showed several interesting features. Near the bed, maximum Reynolds stress was in phase with one of the two peaks of turbulence intensity but further out it was in phase with the other, i.e. the phase of maximum Reynolds stress showed a 180° phase shift at a certain height above the bed. A related effect was seen in the time-mean eddy viscosity which was negative near the bed but positive further out. It is suggested that these effects are caused by the jets of fluid associated with vortex formation and ejection in oscillatory flow over rough beds. Maximum Reynolds stress was also significantly less than the horizontal force per unit area of bed obtained from the momentum integral. Eddy viscosity and mixing length were found to vary significantly during the course of the cycle. Variation with height of time-mean values of these variables showed similar trends, except in the near-bed region, to those observed in steady flow but derived values of the Kármán constant were significantly lower. Non-dimensional defect velocity appeared to show dependence on a/k_s as well as on y/δ in the outer layer away from the bed, even at high Reynolds numbers.

1. Introduction

A great many models have been proposed for turbulent boundary layers in oscillatory flow. Amongst others, Jonsson (1963, 1980), Kajiura (1968), Johns (1975, 1977), Bakker (1974), Brevik (1981) and Fredsoe (1981*b*) have investigated purely oscillatory boundary layers, and Lundgren (1972), Smith (1977), Bakker & Van Doorn (1978), Grant & Madsen (1979), Tanaka & Shuto (1981), Fredsoe (1981*a*, 1982) and Christofferson (1982) have considered the combined effect of waves and currents.

All of these theoretical models make assumptions about the characteristics of turbulence in oscillatory flow. The experimental support for many of these assumptions is weak. Although there have been quite a number of velocity measurements in oscillatory boundary layers (e.g. Kalkanis 1957, 1964; Jonsson 1963; Horikawa & Watanabe 1968; Sleath 1970, 1982; Jonsson & Carlsen 1976; Van Doorn 1981), there have been relatively few direct measurements of the turbulence characteristics. In this respect, the most significant contributions are those of Kemp & Simons (1982, 1983) who made one-component velocity measurements for waves and currents and Hino *et al.* (1983) who investigated oscillatory flow over smooth walls.

The object of the present paper is to provide more experimental data with which to test the hypotheses on which the various models are based. Only pure oscillatory flow over rough beds is considered. Although measurements were made over quite a wide range of flow conditions, attention is concentrated on the tests with the highest Reynolds numbers for which the turbulence was, hopefully, fully developed. The question of transition to turbulence will be considered elsewhere.

2. Experimental arrangement

The experiments were carried out in an oscillatory-flow water tunnel. This tunnel was the same as that described by Du Toit & Sleath (1981) except that the central panels of Perspex were replaced by plate glass. The working section was 0.305 m wide, 0.45 m high and 3.66 m long. The oscillatory flow was maintained close to its resonant period of 4.5 s by a paddle in one arm of the tunnel driven by a variable-speed motor with feedback control. Because of the linkage mechanism driving the paddle, the free-stream flow in the test section was not pure simple harmonic. However, the amplitude of the second harmonic was always less than 3 % of the fundamental and the third harmonic was less than 1 %.

The velocity distribution in the boundary layer was measured for four different rough beds. These consisted of a single layer of sand, gravel or pebbles of median diameters 0.20, 1.63, 8.12 and 30.0 mm and standard deviations 0.06, 0.52, 3.36 and 3.02 mm, respectively. The 8.12 mm gravel consisted of granite chippings and was very angular whereas the 30.0 mm pebbles were rounded. The two sands were intermediate in shape between these two extremes. The 30.0 mm pebbles were laid directly on the floor of the water tunnel but the other three sediments were glued to flat plates. This was achieved by diluting a contact adhesive with petrol. The glue was then spread uniformly over the surface of the plate and the sediment poured on top. When the glue was dry the excess sediment was tipped off and the plates were fixed rigidly to the bottom of the water tunnel. Each rough bed consisted of three plates, each of length 1.22 m and width 0.30 m, laid end to end. The junction between pairs of plates was scraped clean of sediment, taped over, covered with glue, and then re-sprinkled with a single layer of sediment. The same procedure was followed for the screw heads which were countersunk into the plate.

The velocities were measured with a laser-Doppler anemometer. A 15 mW Helium–Neon laser was used in forward-scatter mode with a Malvern Instruments frequency shifter. Two velocity components were measured by splitting one of the two beams emerging from the frequency shifter with a DISA polarizing beam splitter. This provided two beams polarized at 90° to each other and at +45° and −45° to the other beam from the frequency shifter. Appropriately adjusted polarizing filters on the two photomultipliers thus allowed separation of the horizontal and vertical components of velocity. It was the need to maintain correct polarization of the three beams that led to the replacement of the Perspex panels by plate glass, mentioned above. As with the experiments of Du Toit & Sleath (1981) the measuring volume was 0.3 mm wide, 0.3 mm high and 1.0 mm across the tunnel. The laser, optics and photomultipliers were mounted on a milling-machine base which could be traversed vertically and horizontally. Output from the photomultipliers was passed through two frequency trackers and an analog-to-digital converter directly to a BBC microcomputer. In general, a Cambridge Consultants frequency tracker was used for the horizontal component of velocity and a DISA tracker for the vertical velocity. Periodic tests

were carried out with the trackers the other way round to ensure that they both gave the same output.

As mentioned above, the period of oscillation was close to 4.5 s in all of the tests. Consequently a fixed sampling rate was used corresponding to approximately 190 samples per cycle. This was sufficiently slow to allow direct online determination of the turbulence parameters and mean velocities. Sampling was triggered by a phase marker attached to the flywheel of the motor driving the paddle. For the rough beds consisting of the two sands, 200 cycles were analysed at each measuring point. For the gravel and pebble beds only 100 cycles were analysed at each point. This was because the rougher bed required measurements at several (usually between four and seven) horizontal positions in order to obtain a reasonable average for any given vertical position. Most of the results presented below for the two rougher beds represent the average for the various horizontal positions. Preliminary tests were carried out with the pebble bed to determine the minimum number of cycles required for consistent results at any given measuring position. These indicated that for record lengths greater than about 50 cycles there was no significant improvement in the consistency of the measurements with increase in the number of cycles sampled.

Because of the limited storage capacity of the BBC microcomputer it was not feasible using the above techniques to obtain satisfactory power spectra of the velocity fluctuations. Consequently, a number of measurements were made with output from the laser-Doppler anemometer recorded directly on magnetic tape using a Racal Store 4 analog instrumentation recorder. These recordings were then played back into a Hewlett Packard 5420B Digital Signal Analyser to obtain the desired spectra. Spectra were obtained at given phases through the cycle by means of the phase marker signal and a variable time delay. Once triggered, 1024 samples were taken at a rate of 3280 Hz. 50 cycles were sampled in this way and the results at each phase were averaged to produce the final spectra.

The usual test procedure was as follows. The water in the tunnel was adjusted to the appropriate level and the motor was set in motion with the desired period and amplitude of oscillation. Electronic equipment was also switched on. After approximately four hours, when conditions were judged to be steady, water temperature and period of oscillation were recorded. Measurements were then made at the required positions of the velocity components normal to the bed and parallel to the direction of oscillation. At least one set of measurements was made in the free stream, well away from the bed. This was usually the last position to be sampled but, for some tests, was sampled at the beginning of the test as well. Finally, water temperature and period of oscillation were measured again.

3. Dimensional analysis

It will help in the interpretation of the experimental results if we list the relevant dimensionless groups. We take the independent variables to be y, the distance measured vertically up from the mean crest level of the bed roughness, U_0, the amplitude of the fluid velocity outside the boundary layer, a, the orbital amplitude of fluid particles outside the boundary layer, k_s, the Nikuradse roughness size, ν, the kinematic viscosity. Thus, any dependent variable may be expressed as a function of

$$\frac{y}{k_s}, \quad \frac{U_0 a}{\nu}, \quad \frac{a}{k_s}.$$

Since the boundary-layer thickness δ is defined as the value of y at a given value of defect velocity divided by U_0 we have

$$\frac{\delta}{k_s} = f\left(\frac{U_0 a}{\nu}, \frac{a}{k_s}\right). \tag{1}$$

Thus, without loss of generality, we may replace y/k_s by y/δ. Also, it may be argued that outside the viscous sublayer the defect velocity and hence turbulence intensity are independent of viscosity. Thus, in this defect layer,

$$\frac{\hat{u}_d}{U_0} = f\left(\frac{y}{\delta}, \frac{a}{k_s}\right), \quad \frac{(\overline{u'^2})^{\frac{1}{2}}}{U_0} = f\left(\frac{y}{\delta}, \frac{a}{k_s}\right), \tag{2}$$

where u_d is the defect velocity, a circumflex denotes amplitude, and an overbar denotes a time-mean value. Finally, since the ratio of the amplitude of the friction velocity $\hat{u}_*$ to U_0 is also a function of y/δ and a/k_s if the constant-stress layer extends beyond the viscous sublayer, we may also write

$$\frac{\hat{u}_d}{\hat{u}_*} = f\left(\frac{y}{\delta}, \frac{a}{k_s}\right). \tag{3}$$

4. Test conditions

The test conditions are summarized in table 1.

The friction coefficient f_w is defined as

$$f_w = \frac{\hat{\tau}_0}{\frac{1}{2}\rho U_0^2}, \tag{4}$$

where τ_0 is the value of the shear stress τ at the mean level of the grain crests and ρ is the fluid density. The value of f_w given in table 1 is that obtained with τ defined as

$$\tau = \rho \int_y^\infty \frac{\partial(u_\infty - u)}{\partial t} \mathrm{d}y \tag{5}$$

where u_∞ is the value of u outside the boundary layer. The difference between the value of f_w obtained in this way and that given by $2\rho\hat{u}_*^2/U_0^2$ will be discussed below.

The roughness length k_s is taken equal to $2D$ and the friction velocity is $u_* = (-\overline{u'v'})^{\frac{1}{2}}$.

5. Turbulent fluctuations in velocity

Since the main object of this paper is to investigate the effects of turbulence, we shall start with this question and postpone a discussion of the mean-velocity profiles until later.

Figure 1 shows an example of how the root-mean-square fluctuation in the horizontal component of velocity varies during the course of the cycle at various heights above the grain crests. Phase is measured relative to maximum negative velocity in the free stream. Thus, the free-stream velocity is minimum at 0°, maximum at 180°, and zero at −90° and +90°. For each phase, u' is the fluctuation in velocity relative to the mean of the 200 samples taken at that phase.

Figure 2 shows the equivalent records for the root-mean-square fluctuation in the vertical velocity. In both figures it is clear that the variation in turbulence intensity during the course of the cycle is significant, particularly near the bed.

The way in which $\overline{u}_{rms}$, the mean value of $(\overline{u'^2})^{\frac{1}{2}}$ over the whole cycle, varies with

Test no.	Period (s)	U_0 (m/s)	$\nu \times 10^6$ (m^2/s)	a/k_s	$\hat{u}_*$ (m/s)	$\frac{\hat{u}_*}{\bar{u}_*}$	f_w	δ mm	No. of cycles sampled at each position
				0.20 mm sand					
1	4.49	0.623	1.10	1112	0.0128	—	0.00452	14.4	200
2	4.49	0.417	1.10	743	0.0047	—	0.00599	—	200
				1.63 mm sand					
3	4.54	0.686	1.21	151	0.0226	1.73	0.0161	23.5	200
4	4.58	0.617	1.19	138	0.0204	1.66	0.0158	23.5	200
5	4.48	0.490	1.16	115	0.0170	1.79	0.0172	19.5	200
6	4.59	0.326	1.16	72.9	0.0123	1.79	0.0260	14.7	200
7	4.51	0.228	1.13	50.1	0.0059	—	0.0330	9.3	200
8	4.52	0.113	1.14	24.8	—	—	—	7.9	200
				8.12 mm gravel					
9	4.55	0.621	1.19	27.7	0.0224	1.35	0.0270	35.4	100
10	4.50	0.487	1.17	21.5	0.0182	1.35	0.0381	34.1	100
11	4.50	0.178	1.19	7.87	0.0074	1.35	0.0880	27.4	100
12	4.49	0.106	1.16	4.67	0.0047	—	0.136	—	100
13	4.47	0.053	1.16	2.34	0.0020	—	—	—	100
				30.0 mm pebbles					
14	4.60	0.712	1.21	8.69	0.0372	1.61	0.0451	48.6	100
15	4.53	0.582	1.20	6.98	0.0317	1.58	0.0572	48.6	100
16	4.55	0.357	1.19	4.30	0.0141	1.28	0.103	48.2	100
17	4.56	0.097	1.16	1.17	0.0054	—	—	28.2	100
18	4.53	0.062	1.13	0.74	0.0025	—	—	15.0	100
19	4.52	0.630	1.18	7.69	0.0337	—	—	—	100

TABLE 1. Test conditions

height is shown for the four different beds in figure 3. The corresponding results for $\overline{v}_{rms}$ are given in figure 4. To avoid confusion, and also because the object of the present paper is to investigate fully established turbulence, only the three tests with the largest Reynolds numbers are shown for the three roughest beds and only the largest Reynolds number is shown for the 0.2 mm sand. Once again, y is measured from the mean level of the grain crests. It could be argued that y ought really to be measured from some mean bed level. For example, Einstein (1950) suggested that the origin should be taken $0.35D$ below the crest level. In the present case this would make little difference to the overall level of scatter shown by the different curves although it would, of course, produce a significant shift in origin for the rougher beds.

The boundary-layer thickness δ in these figures is that measured from the grain crests out to the point at which the amplitude of the defect velocity is 5 % of U_0. A more common definition for the edge of the boundary layer would be the point where the defect velocity is 1 % of U_0. The defect velocity was obtained in these experiments by subtracting the free-stream velocity phase by phase from the velocity at each level. Inevitably there was some fluctuation in the period of oscillation between the time when the measurements at any given level were made and the time (at the end of the test) when the free-stream velocity was recorded. From the duplicate measurements of free-stream velocity made at the start of a number of the tests it was judged that the defect velocity was not reliable when it fell below about $0.03U_0$. It was for this reason that the 5 % limit was adopted for δ.

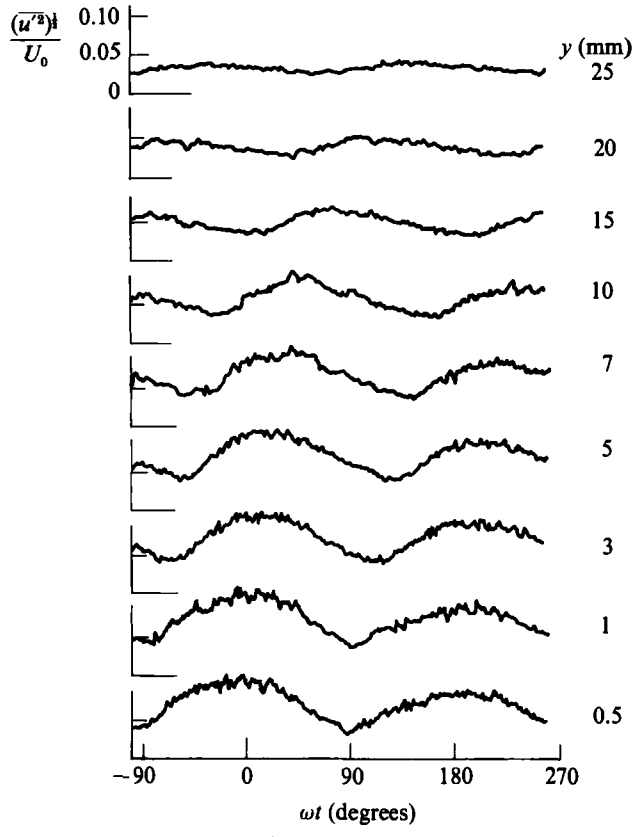

FIGURE 1. Variation of $(\overline{u'^2})^{\frac{1}{2}}$ during the course of the cycle: Test no. 4.

The measurements in figures 3 and 4 show very similar trends to those observed in steady flows. For the bed of 0.2 mm sand, which approximates most closely to a smooth bed, both $\overline{u}_{\text{rms}}$ and $\overline{v}_{\text{rms}}$ rise to a maximum and then decline with increasing distance from the bed. The maximum in $\overline{u}_{\text{rms}}$ occurs closer to the bed than that for $\overline{v}_{\text{rms}}$ as observed for steady flows (see e.g. Klebanoff 1954). The maximum value of $\overline{u}_{\text{rms}}$ is also significantly larger than that for $\overline{v}_{\text{rms}}$. As bed roughness increases, values of $\overline{u}_{\text{rms}}$ and $\overline{v}_{\text{rms}}$ also increase for any given y/δ as observed for steady flows by Corrsin & Kistler (1954).

Figures 5 and 6 show the magnitude of the fluctuations in $(\overline{u'^2})^{\frac{1}{2}}$ and $(\overline{v'^2})^{\frac{1}{2}}$ during the course of a half-cycle. The quantity $\Delta(\overline{u'^2})^{\frac{1}{2}}$ is the difference between the average of the two maxima and the average of the two minima of $(\overline{u'^2})^{\frac{1}{2}}$ during the course of a cycle, and similarly for $\Delta(\overline{v'^2})^{\frac{1}{2}}$. The overall trends appear to be much the same as those for the mean values of the turbulence intensities. The value of $\Delta(\overline{v'^2})^{\frac{1}{2}}$ rises to a maximum and then declines steadily with increasing y/δ. For $\Delta(\overline{u'^2})^{\frac{1}{2}}$ the initial rise is less clear but otherwise the trend is the same.

In these figures there is considerable scatter between the results for different tests, particularly for the roughest bed. This is probably due in part to the difficulty of obtaining a true average from point measurements in highly three-dimensional flows. Figure 7 shows measurements made at a fixed height of 3 mm above the grain crests for the 30.0 mm pebbles. In this figure x is distance measured horizontally in the direction of oscillation from some arbitrary origin. It is clear that there is very

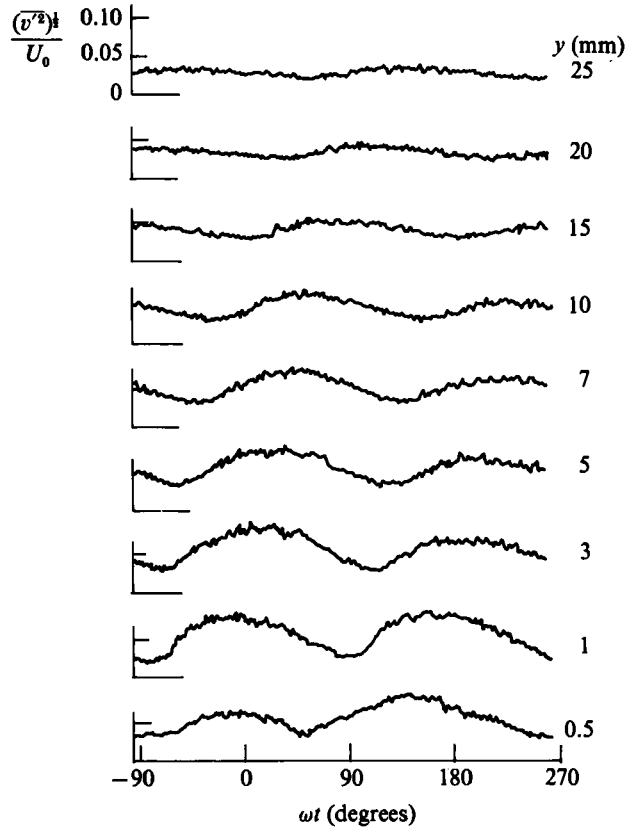

FIGURE 2. Variation of $(\overline{v'^2})^{\frac{1}{2}}$ during the course of the cycle: Test no. 4.

significant spatial variation in the turbulence intensity at any given height. As mentioned above, the results for the two rougher beds in figures 3–6 represent the average of measurements at several values of x for each height y. These values of x were equally spaced between $x = 40$ and 130 mm. Clearly a great many measurements at each height would be required to obtain a true average. Figure 7 represents the worst case from this point of view. The three-dimensionality of the flow was significantly less for the 8.12 mm gravel and negligible for the other two beds.

The variation in velocity with horizontal position shown in figure 7 has several causes. One is the variability in the effective bed level because of the random arrangement and shape of the pebbles making up the bed. It is clear from figures 3–6 that an effective variation in y could produce significant change in turbulence intensity. This is probably the reason why low $\overline{u}_{\mathrm{rms}}$ tends to correlate with high $\hat{u}$ in figure 7 since, in the vicinity of $y = 3$ mm, $\hat{u}$ increases while $\overline{u}_{\mathrm{rms}}$ decreases with distance from the bed. A second cause of variability is the formation of vortices by the individual roughness elements. Since vortex formation and ejection are strongly dependent on U_0, the intensity of turbulence at a given point might be expected to vary from one test to another.

Another cause for differences between the results for different tests in figures 3–6 is the effect of relative roughness. Figure 8 shows how the maximum value of the various turbulence intensities varies with the roughness parameter a/k_s. Following the argument outlined in §3, these maximum intensities will, in general, be functions

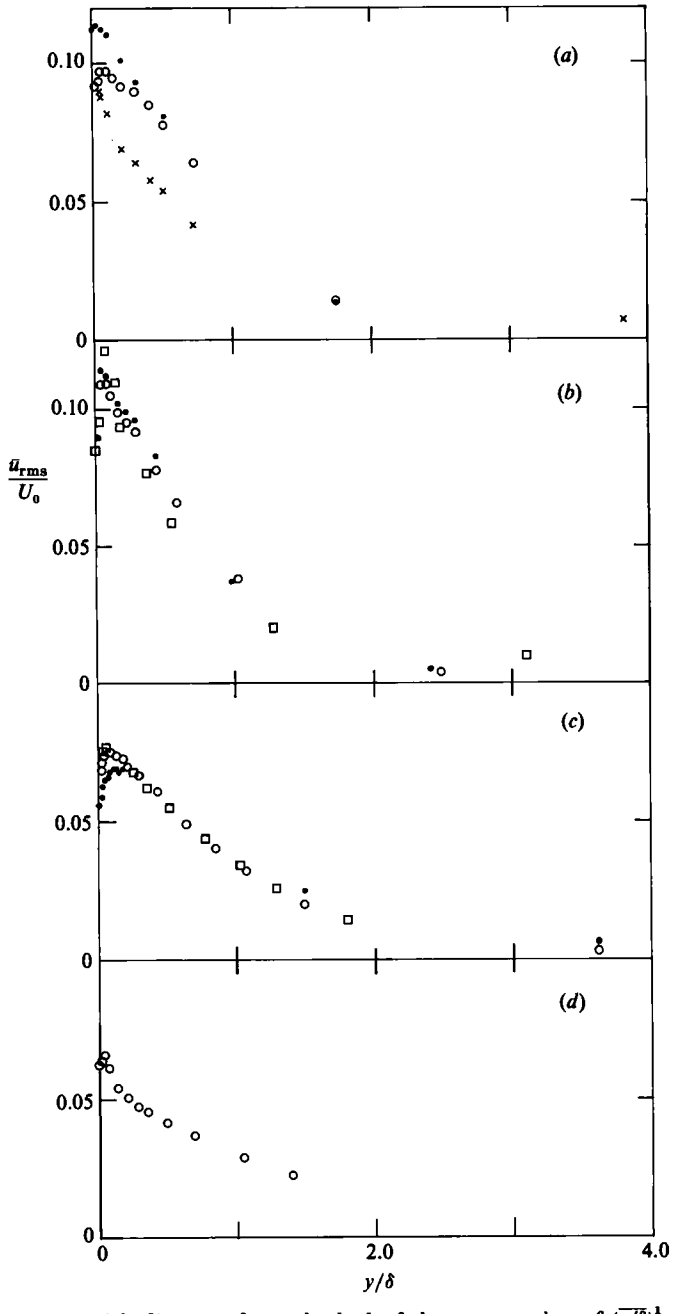

FIGURE 3. Variation with distance from the bed of the mean value of $(\overline{u'^2})^{\frac{1}{2}}$ during the course of a cycle. (*a*) $D = 30.0$ mm: ●, Test no. 14 (0.712 m/s); ○, Test no. 15 (0.582 m/s); ×, Test no. 16 (0.357 m/s). (*b*) $D = 8.12$ mm: ○, Test no. 9 (0.621 m/s); ●, Test no. 10 (0.487 m/s); □, Test no. 11 (0.178 m/s). (*c*) $D = 1.63$ mm: ○, Test no. 3 (0.686 m/s); ●, Test no. 4 (0.617 m/s); □, Test no. 5 (0.490 m/s). (*d*) $D = 0.20$ mm: ○, Test no. 1 (0.623 m/s). The numbers in brackets after the Test nos are the values of U_0.

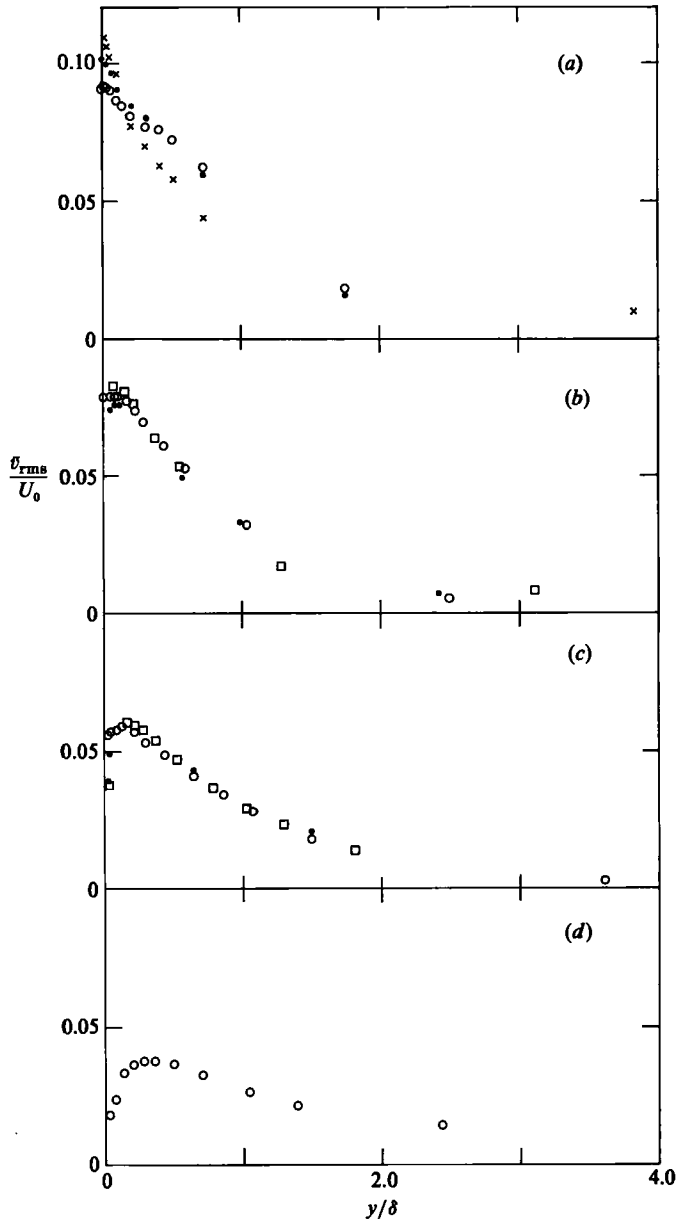

FIGURE 4. Variation with distance from the bed of the mean value of $(\overline{v'^2})^{\frac{1}{2}}$ during the course of a cycle. Symbols as for figure 3.

of $U_0 a/\nu$ as well as a/k_s. However, at sufficiently large values of $U_0 a/\nu$ we expect Reynolds-number dependence to be negligible. In fact, the results for the various beds do appear to tend towards unique curves in figure 8 at the highest values of $U_0 a/\nu$.

Figure 8 shows that the peak values of $\Delta(\overline{u'^2})^{\frac{1}{2}}$ and $\Delta(\overline{v'^2})^{\frac{1}{2}}$ remain more or less constant with increasing a/k_s whereas the peak values of $\overline{u}_{\text{rms}}$ and $\overline{v}_{\text{rms}}$ decrease steadily (at sufficiently high Reynolds numbers). In other words, the fluctuation in turbulence intensity during the course of the cycle becomes less important relative to the mean level of turbulence intensity as bed roughness increases. It would also

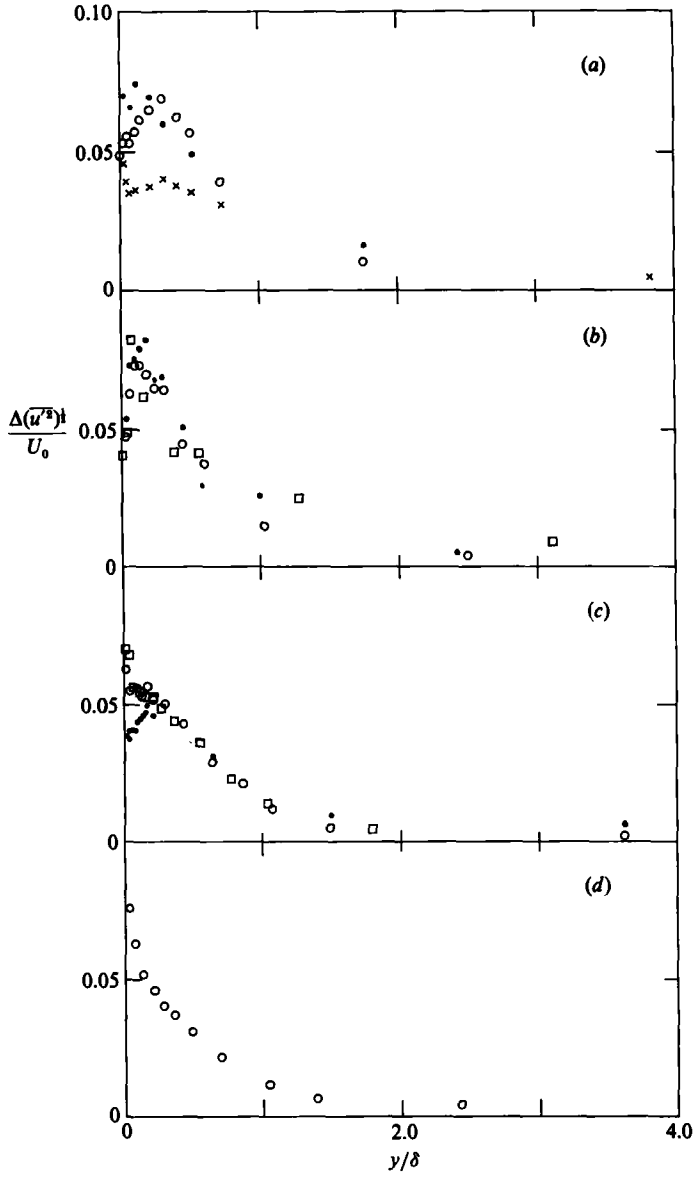

FIGURE 5. Variation with distance from the bed of the magnitude of the fluctuation in $(\overline{u'^2})^{\frac{1}{2}}$ during the course of a cycle. Symbols as for figure 3.

seem that the difference between $\overline{u}_{\text{rms}}$ and $\overline{v}_{\text{rms}}$ also decreases as bed roughness increases. This may be because the dampening effect on vertical perturbations in velocity becomes less significant when the bed approximates less to a horizontal plane.

It is also interesting to examine the phase at which the turbulence intensity is greatest at any given height above the bed. This is shown by figure 9 for $(\overline{v'^2})^{\frac{1}{2}}$. In this figure the same straight line has been drawn through each set of test results. This line is that which gave the best fit to the experimental results for the phase of $(\overline{u'^2})^{\frac{1}{2}}$ for the bed of 1.63 mm sand. It is included in figure 9 only to facilitate comparison between the results for different beds.

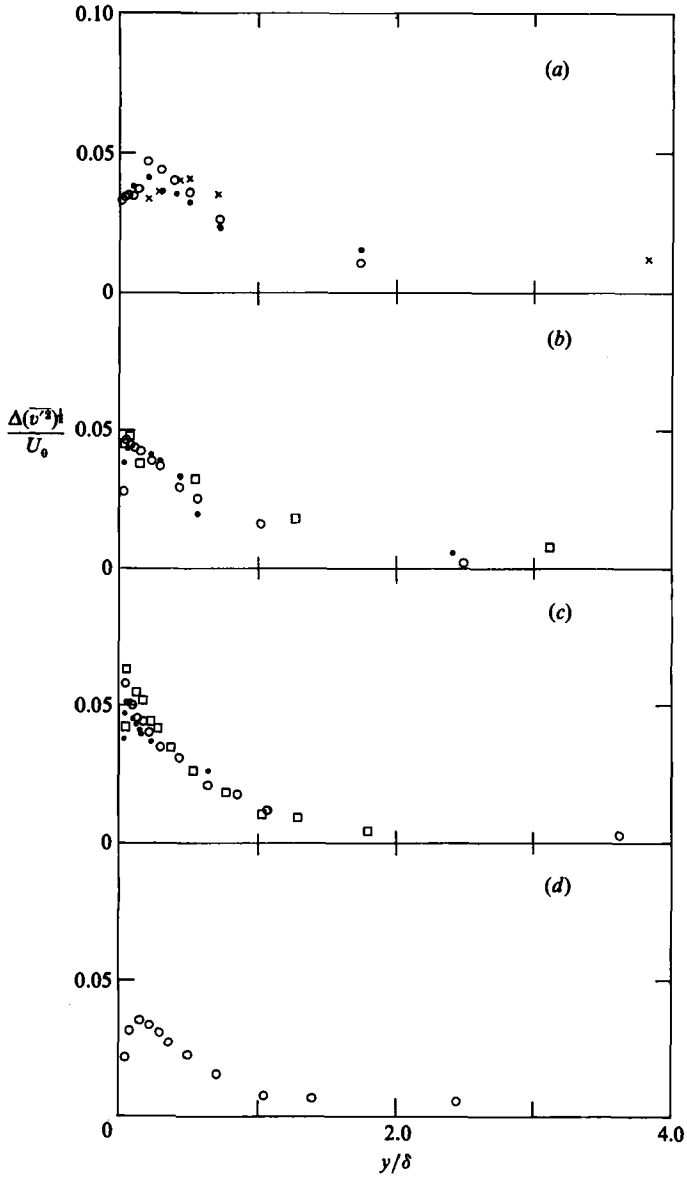

FIGURE 6. Variation with distance from the bed of the magnitude of the fluctuation in $(\overline{v'^2})^{\frac{1}{2}}$ during the course of a cycle. Symbols as for figure 3.

Very similar results are obtained for the phase at which $(\overline{u'^2})^{\frac{1}{2}}$ is maximum. These results are not shown here in order to reduce the length of the paper. Although the experimental scatter is considerable it would seem that the maximum value of $(\overline{v'^2})^{\frac{1}{2}}$ occurs at more or less the same time as the maximum of $(\overline{u'^2})^{\frac{1}{2}}$ and that these maxima propagate up from the bed at more or less the same speed regardless of bed roughness. The straight line corresponds to

$$\frac{\mathrm{d}(\omega t)}{\mathrm{d}(y/\delta)} = 2.27 \text{ rad}, \tag{6}$$

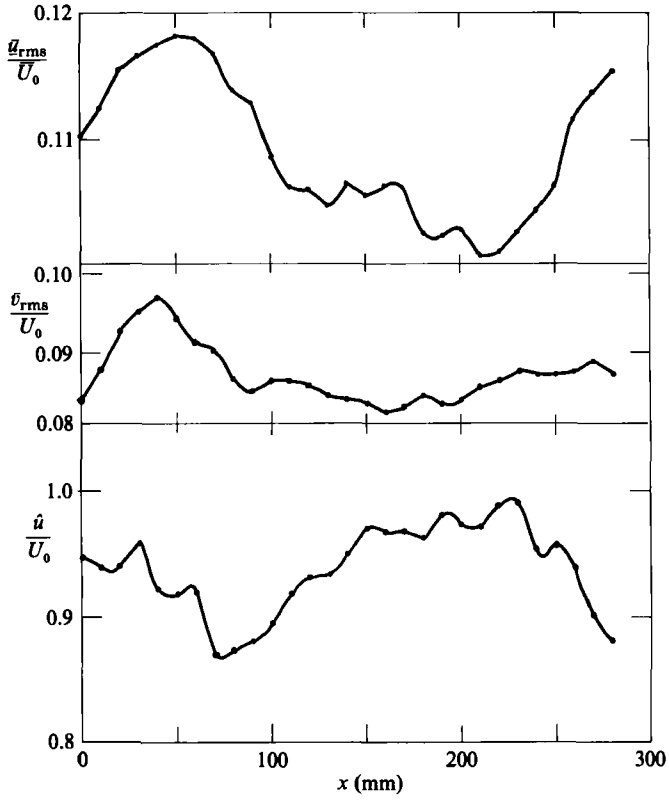

FIGURE 7. Variation with horizontal position of the amplitude of u and of the mean values of $(\overline{u'^2})^{\frac{1}{2}}$ and $(\overline{v'^2})^{\frac{1}{2}}$. Test no. 19 ($y$ = 3 mm).

where ω is the angular frequency of oscillation ($=2\pi/T$, where T is the period of oscillation). Thus

$$\text{upward propagation velocity} \doteq \frac{\omega\delta}{2.27}.$$

This propagation of the maximum turbulence intensity away from the bed is also clearly shown by the turbulence-intensity contours. Figure 10 gives a typical example.

It is of interest to speculate what triggers the increase in turbulence during each half-cycle. Figure 11 shows the phase at which maximum turbulence occurs for one of the tests with the 1.63 mm sand. Also shown is the phase at which the velocity is maximum. Various investigators (e.g. Hino *et al.* 1983) have drawn attention to the way in which turbulence intensity increases during the deceleration stage of each half-cycle and then decreases when the fluid starts to accelerate again. On that basis the maximum turbulence intensity would occur during the quarter-cycle following maximum velocity. The results in figure 11 show that this is so for small values of y/δ but not when y/δ exceeds about 0.7. It follows that under this hypothesis the turbulence would be generated in the region close to the bed and would then propagate freely upward.

Many writers have drawn attention to the instability associated with a point of inflexion in the velocity profile. Figure 11 shows the phase at which $\partial^2 u/\partial y^2 = 0$. The

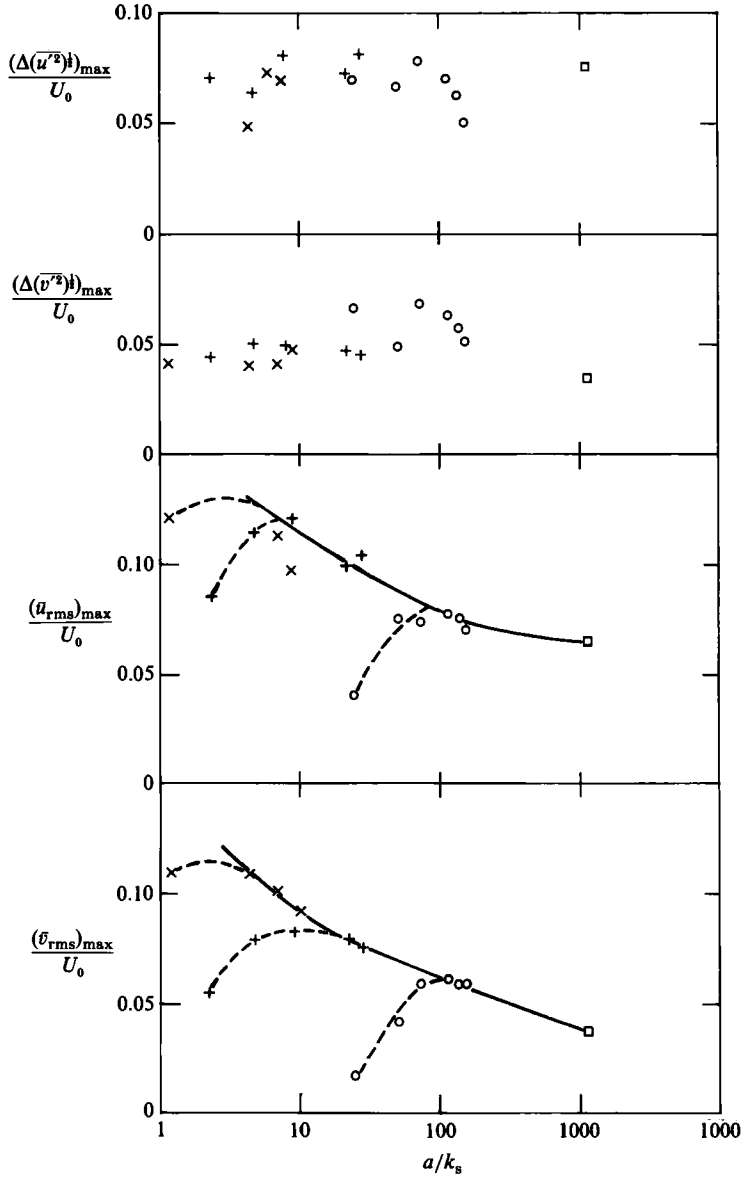

FIGURE 8. Variation with a/k_s of the peak values shown by the curves of $\Delta(\overline{u'^2})^{\frac{1}{2}}$, $\Delta(\overline{v'^2})^{\frac{1}{2}}$, $\overline{u}_{rms}$ and $\overline{v}_{rms}$ versus height.

correlation with maximum turbulence intensity is reasonably close, but by no means perfect, and extends over a fairly wide range of y/δ. Equally good correlation is shown with the maximum of the defect velocity but this may be because it is the turbulence that drives the defect velocity rather than vice versa. An alternative explanation for what produces the fluctuation in turbulence intensity will be put forward in § 10.

Finally, figure 12 shows power spectra for the fluctuations in velocity at various phases in the cycle. Each curve covers a range of phase because, as explained above, the sampling takes place over a finite interval of time (0.31 s in each case). These spectra are similar to those obtained for smooth beds by Hino *et al.* (1983) except

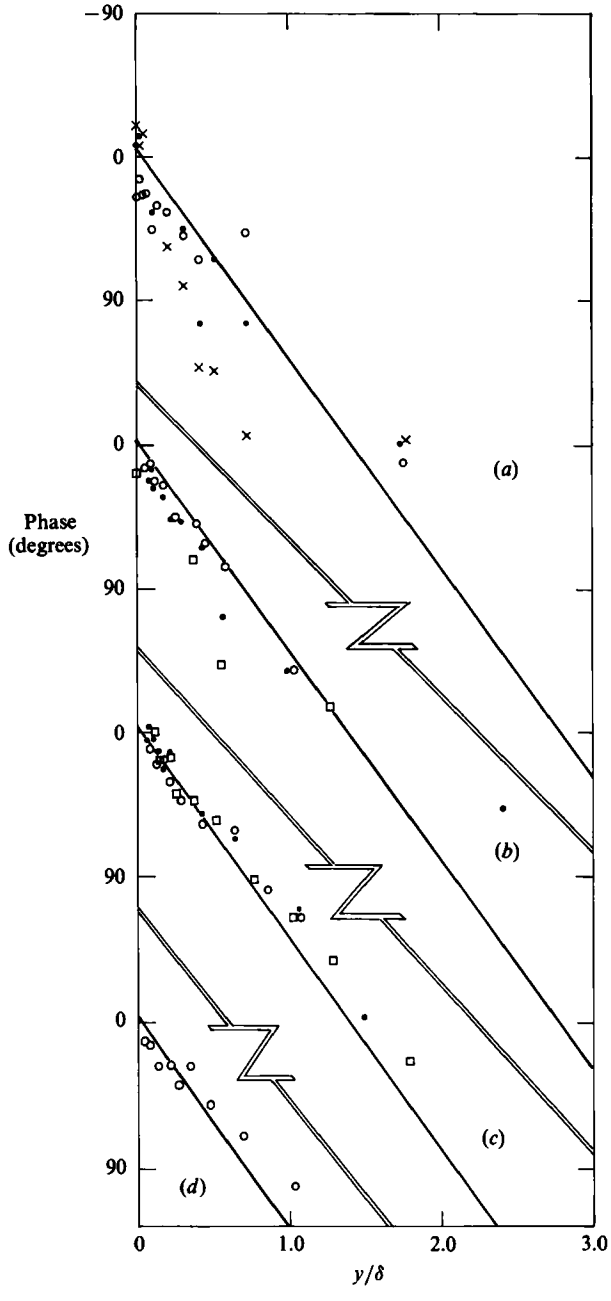

FIGURE 9. Variation with height of the phase of the peak value of $(\overline{v'^2})^{\frac{1}{2}}$, (*a*) $D = 30.0$ mm: ○, Test no. 14; ●, Test no. 15; ×, Test no. 16. (*b*) $D = 8.02$ mm: ●, Test no. 9; ○, Test no. 10; □, Test no. 11. (*c*) $D = 1.63$ mm: ●, Test no. 3; ○, Test no. 4; □, Test no. 5. (*d*) $D = 0.02$ mm: ○, Test no. 1.

that there is no significant difference between the acceleration and deceleration parts of the cycle. On the whole, the spectra have a slope close to that predicted by the $-\frac{5}{3}$ power law except at very low frequencies. However, at these very low frequencies the spectrum is dominated by harmonics of the free-stream velocity. It is, of course,

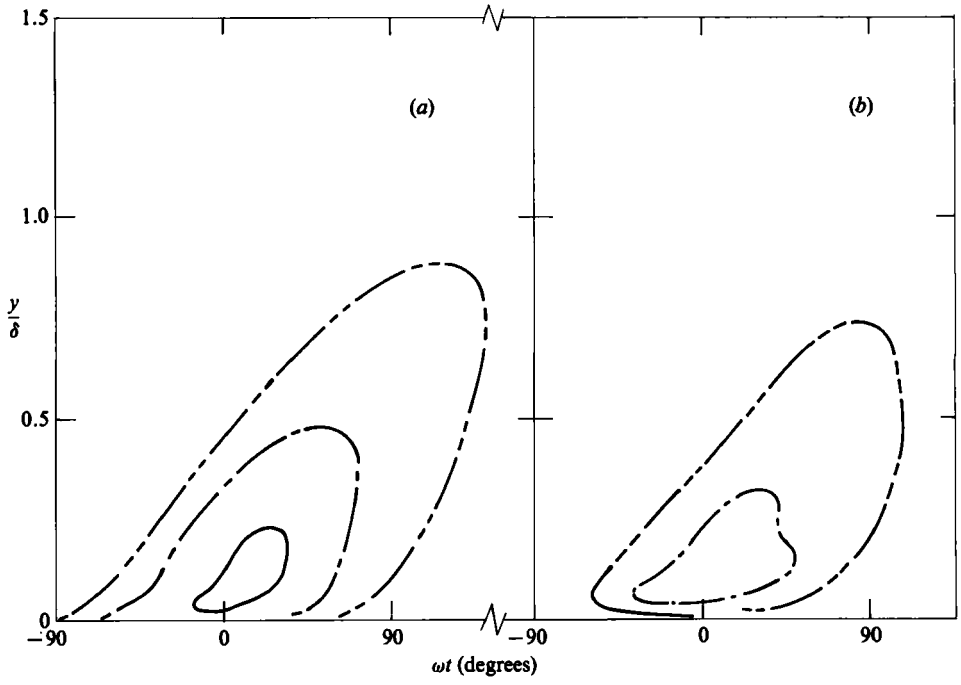

FIGURE 10. Contours of intensity of (*a*) $(\overline{u'^2})^{\frac{1}{2}}/U_0$ and (*b*) $(\overline{v'^2})^{\frac{1}{2}}/U_0$. Values of $(\overline{u'^2})^{\frac{1}{2}}/U_0$ and $(\overline{v'^2})^{\frac{1}{2}}/U_0$ are: ———, 0.05; – – –, 0.075; ——, 0.10: Test no. 4.

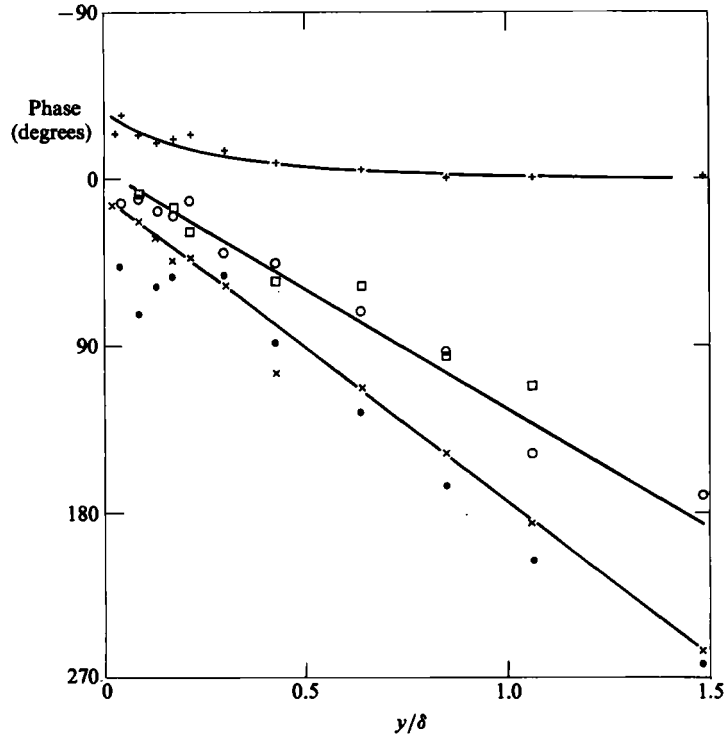

FIGURE 11. Variation of phase with height: +—+, $\hat{u}$; ×—×, $\hat{u}_d$; ○—○, peak $(\overline{u'^2})^{\frac{1}{2}}$; □—□, peak $(\overline{v'^2})^{\frac{1}{2}}$; ●—●, $\partial^2 u/\partial y^2 = 0$: Test no. 4.

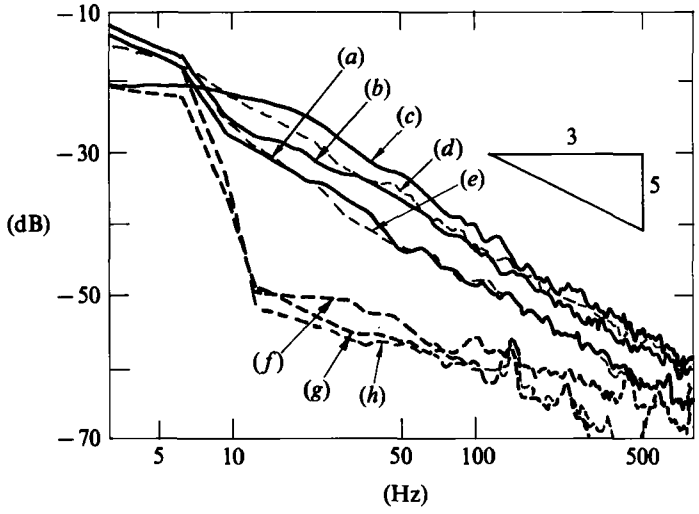

FIGURE 12. Power spectra of fluctuations in horizontal component of velocity. $U_0 = 0.65$ m/s, $T = 4.52$ s, $D = 30.0$ mm. At $y = 4$ mm: (*a*) $-100.7° < \omega t < -75.8°$ ($u/U_0 = 0.21$–0.60); (*b*) $-60.9° < \omega t < -36.0°$ (0.82–1.04); (*c*) $-21.1° < \omega t < 3.8°$ (1.06–0.90); (*d*) $18.7° < \omega t < 43.6°$ (0.70–0.40); (*e*) $58.5° < \omega t < 83.4°$ (0.10–0.30). In free stream: (*f*) $-100.7° < \omega t < -75.8°$; (*g*) $-21.1° < \omega t < 3.8°$; (*h*) $58.5° < \omega t < 83.4°$.

possible that the finite measuring volume of the laser-Doppler anemometer might distort the spectra obtained. However, the comparisons carried out by Hino *et al.* (1983) showed good agreement between the spectra produced by a similar laser-Doppler anemometer and a hot-wire anemometer for frequencies less than about 200 Hz.

6. Shear stress

Figure 13 shows an example of how the non-dimensionalized Reynolds stress varies with time and with distance from the bed. Since the magnitude of the Reynolds stress is very small the quality of the signal is not very good. On the whole, however, we see a more or less sinusoidal variation in Reynolds stress with time.

The phase at which the maximum occurs varies with height as shown in figure 14. These measurements correspond to the maximum of a running average of eight successive samples in order to smooth out high-frequency noise. Each of the four beds shows a similar pattern. Very close to the bed the maximum occurs at 0° (the phase at which the free-stream velocity has its maximum negative value). Initially, the phase lag of the maximum Reynolds stress increases steadily with distance from the bed. However, at a certain height, figure 14 shows a sudden jump in phase of approximately 180°. The transition is not, in fact, quite as sudden as this seems to imply. In figure 13 we see that the 'near-bed' maximum fades gradually into the background as the 'far-bed' maximum becomes established. At $y = 15$ mm, for example, both maxima are visible even though the 'far-bed' maximum (at about −80°) is larger than the 'near-bed' maximum (at about +80°). Even at $y = 20$ mm there is still some trace of the 'near-bed' maximum at a phase of about 90°.

The dashed lines on figure 14 are the same as the solid lines in figure 9. Two dashed lines are shown because $(\overline{u'^2})^{\frac{1}{2}}$ and $(\overline{v'^2})^{\frac{1}{2}}$ show two maxima per cycle. Clearly the

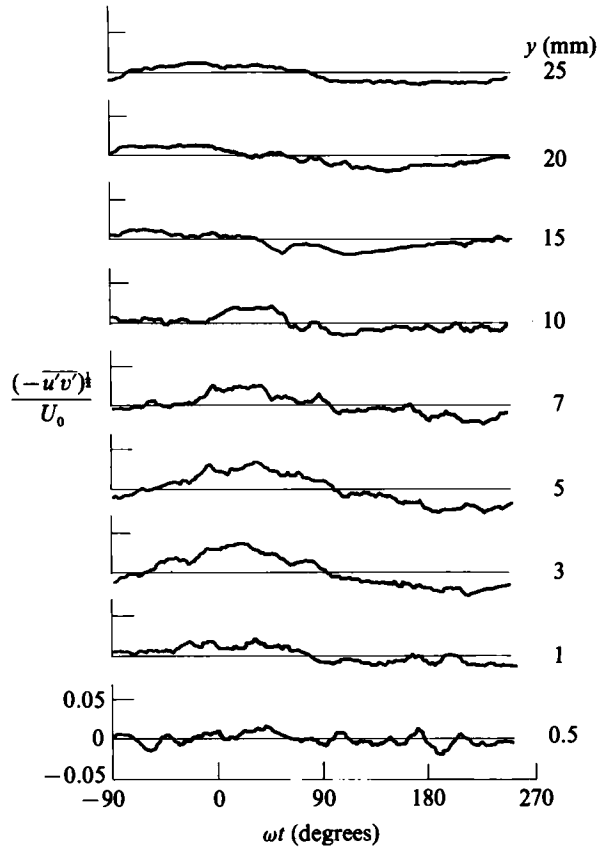

FIGURE 13. Variation of Reynolds stress with phase and height: Test no. 4.

maximum of the Reynolds stress occurs at almost the same phase as the maxima of $(\overline{u'^2})^{\frac{1}{2}}$ and $(\overline{v'^2})^{\frac{1}{2}}$ although the discrepancy increases with distance from the bed. The solid lines in figure 14 (*c*) are the lines of best fit for the experiments with the 1.63 mm sand. The results for the other beds seem to show similar trends but the experimental scatter is too great to allow definite conclusions on this point.

The way in which the amplitude of the Reynolds stress varies with distance from the bed is shown in figure 15. The solid curves are intended only as an indication of the general trend of the experimental results. As might be expected, the amplitude of the Reynolds stress rises to a maximum and then decreases steadily with distance from the bed.

It is interesting to compare these results for Reynolds stress with values of the shear stress given by (5), which has been widely used in flows of this sort. Figure 16 shows an example of how the magnitude of the shear stress calculated from (5) varies with distance from the bed and figure 17 is an example of how its value at $y = 0$ varies with time. Figure 17 also shows the temporal variation in Reynolds stress for the same test at $y = 3$ mm (where the Reynolds stress is maximum). These figures show two interesting features. First, the Reynolds stress and the stress from (5) are almost directly out of phase. This is not unexpected in view of the 180° phase change in the Reynolds stress at larger values of y discussed above. Secondly, the magnitude of the stress given by (5) is much larger than that of the Reynolds stress.

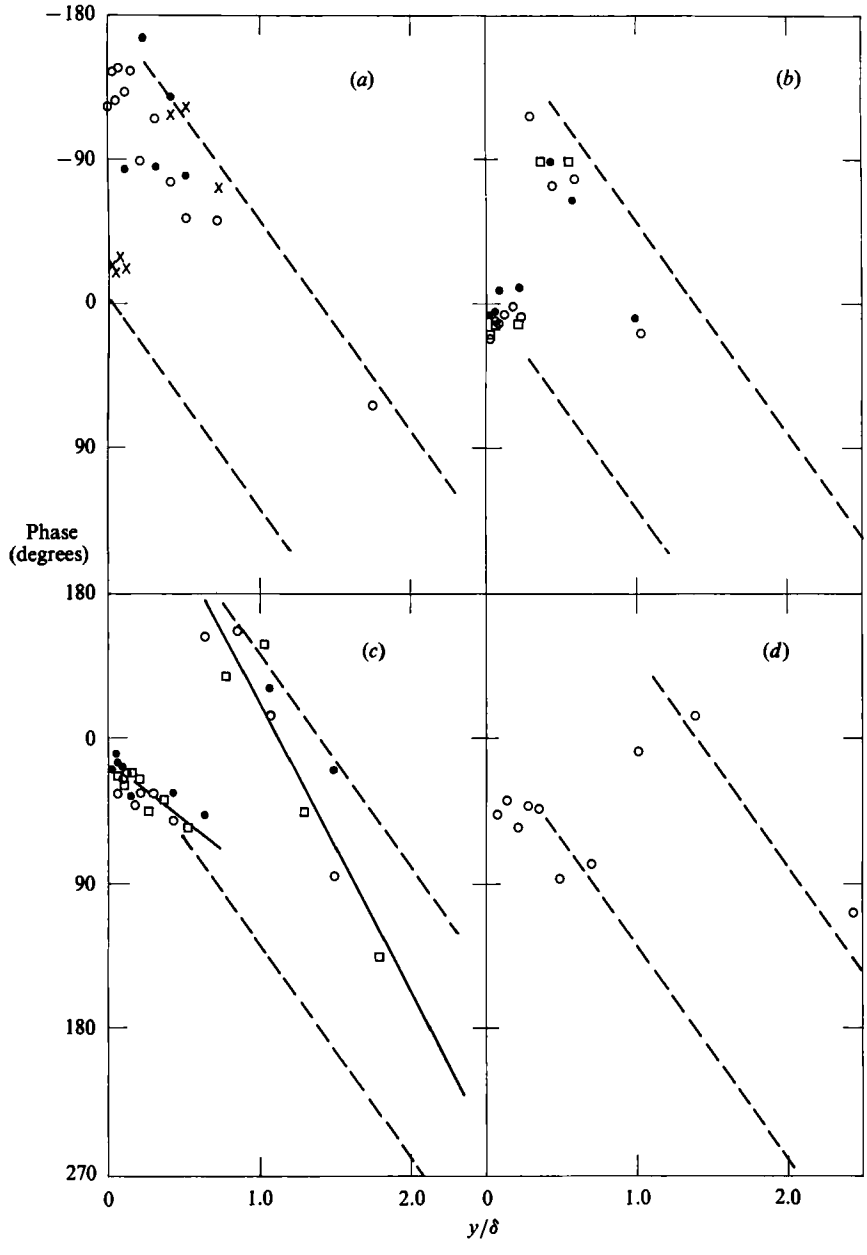

FIGURE 14. Variation with height of the phase of peak Reynolds stress. Symbols as for figure 9.

This second point is seen more clearly in figure 18 which shows values of the friction coefficient f_w, defined by (4), with $\hat{\tau}_0$ calculated from (5) and also with $\hat{\tau}_0$ taken as the maximum value of the Reynolds stress in figure 15. As usual, we assume that the maximum value of the Reynolds stress is equal to the bed stress and that the fall in Reynolds stress as $y \to 0$ is matched by an increase in viscous stress. The line drawn through the values for f_w based on Reynolds stress in figure 18 corresponds to

$$f_w = 0.0067\left(\frac{a}{k_s}\right)^{-0.22}.$$

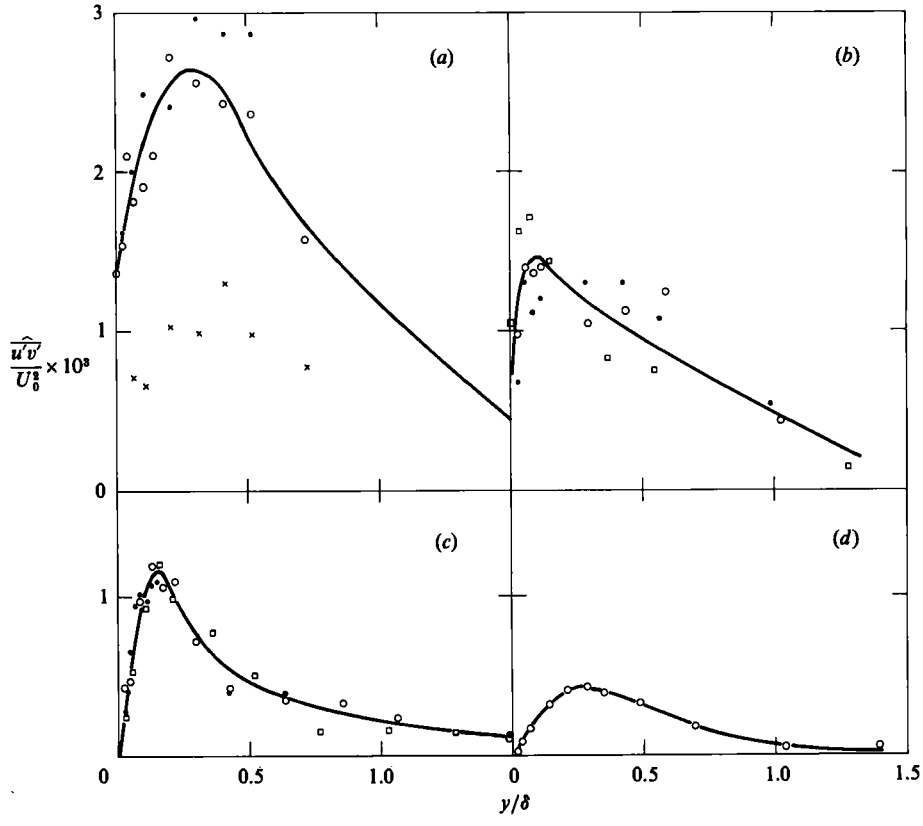

FIGURE 15. Variation of peak Reynolds stress with height. Symbols as for figure 9.

We see that the values of f_w calculated from (5) are between 5 and 10 times those given by the Reynolds stress.

Many authors have pointed out that (5) is inaccurate as a method of measuring turbulent stress. Nevertheless, since the values of f_w calculated from (5) are in good agreement with those of previous investigators, as represented by the empirical curve of Kamphuis (1975) and the semi-empirical curve of Jonsson (1963), it was initially assumed that the present measurements of Reynolds stress must be incorrect. An exhaustive series of checks failed to reveal any malfunction in the equipment or software. However, since it was considered just possible that the three laser beams might not intersect at exactly the same point, thus reducing the correlation of u' and v', it was decided to repeat some of the measurements using the alternative method for measuring Reynolds stress outlined by Kemp & Simons (1983). This makes use of the fact that the Reynolds stress on a horizontal plane is equal to $\frac{1}{2}(\overline{u'^2}-\overline{v'^2})$ on a plane at 45° to the horizontal. To avoid all possibility of cross-talk between the different velocity components, $\overline{u'^2}$ and $\overline{v'^2}$ were measured separately with the third laser beam blanked off. In each case output was taken to the Cambridge Consultants tracker. The results are shown in figure 18. The new measurements give slightly higher values for f_w than before. However, the discrepancy is within the bounds of experimental error since these new measurements involve the small difference between two relatively large quantities.

This still leaves the reason for the very large difference between the Reynolds stress

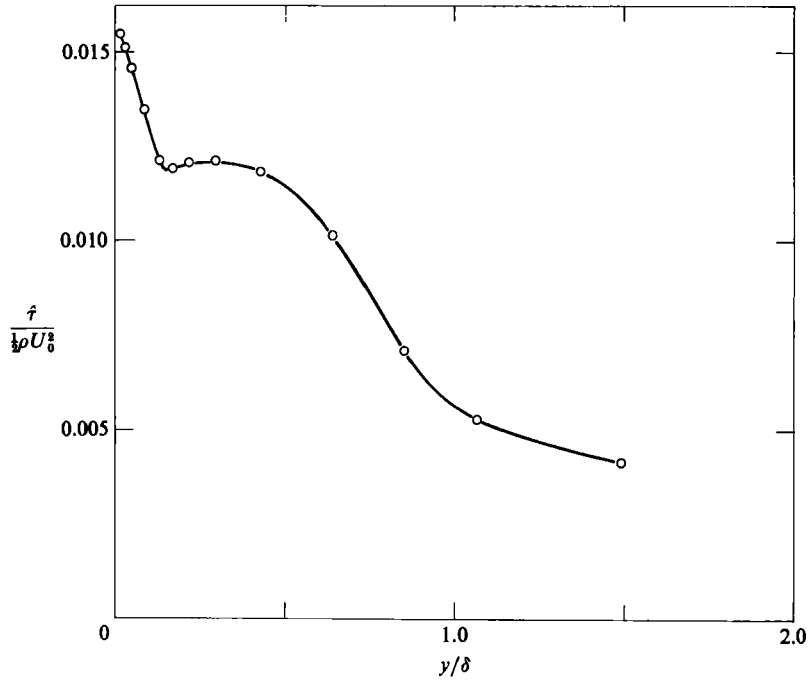

FIGURE 16. Variation with height of the amplitude of shear stress given by (5): Test no. 4.

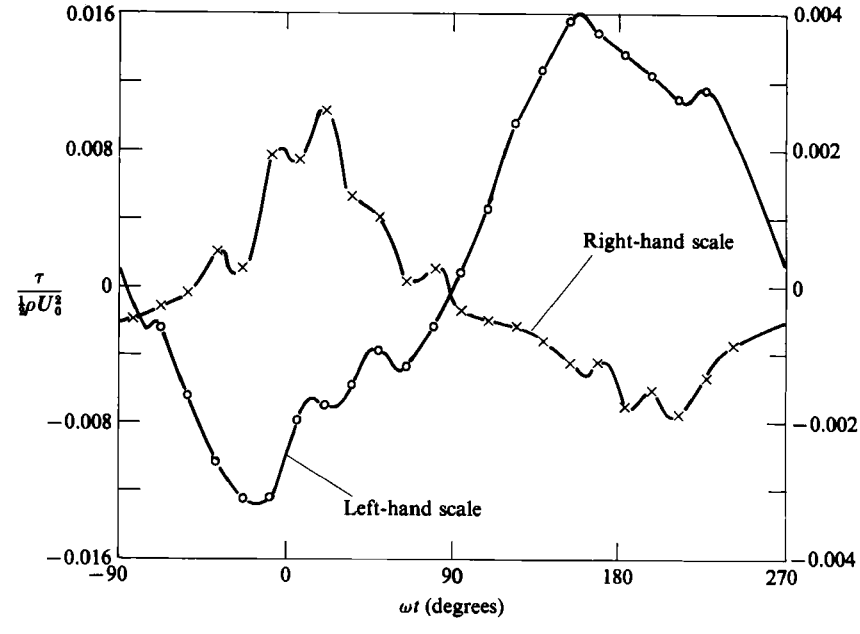

FIGURE 17. Variation during the course of the cycle of the Reynolds stress (×—×) and of the stress given by (5) (○—○); Test no. 4, $y = 3$ mm.

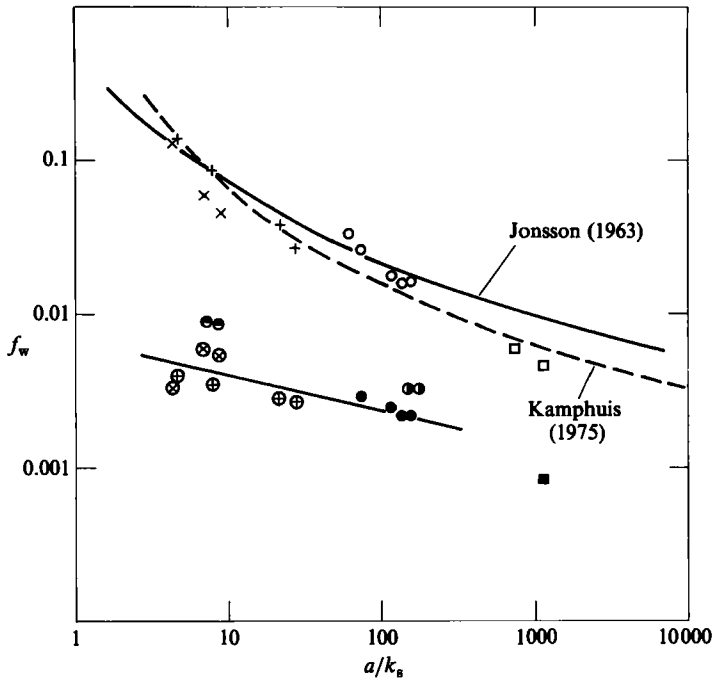

FIGURE 18. Values of friction coefficient. Shear stress given by (5): ×, $D = 30.0$ mm; +, 8.12 mm; ○, 1.63 mm; □, 0.20 mm. Shear stress equal to Reynolds stress: ⊗, $D = 30.0$ mm; ⊕, 8.12 mm; ●, 1.63 mm; ■, 0.20 mm. Shear stress obtained using method of Kemp & Simons (1983): ◓, $D = 30.0$ mm; ◑, 1.63 mm.

and the stress given by (5) unclear. It is suggested in §10, below, that the reason for the discrepancy is that there are significant fluxes of momentum associated with vortex ejection at the end of each half-cycle and that the quantity $\rho\bar{u}\bar{v}$ is far from small. Equation (5) makes no allowance for such an effect and it is also excluded from the Reynolds stress if, as here, the fluctuations u' and v' are measured relative to the mean velocities $\bar{u}$ and $\bar{v}$ at each phase.

7. Eddy viscosity

Most of the models proposed for flow in turbulent boundary layers of this sort have involved assumptions about the eddy viscosity ϵ defined by

$$\tau = \rho\epsilon\frac{\partial u}{\partial y}. \tag{7}$$

Many have assumed the eddy viscosity to be independent of time, for any given height. Figure 19 shows a typical example of how the eddy viscosity at two different heights actually varies during the course of the cycle. In this figure $\bar{\epsilon}$ is the mean value of ϵ during the cycle and τ in (7) is the Reynolds stress. The fact that ϵ is not constant during the cycle has been pointed out by other investigators (e.g. Horikawa & Watanabe 1968). In particular, the singularities when $\partial u/\partial y = 0$ are hardly surprising since the turbulence and hence the Reynolds stress do not instantly disappear as the velocity gradient passes through zero.

Assumptions are also usually made about how the mean value of ϵ during the course

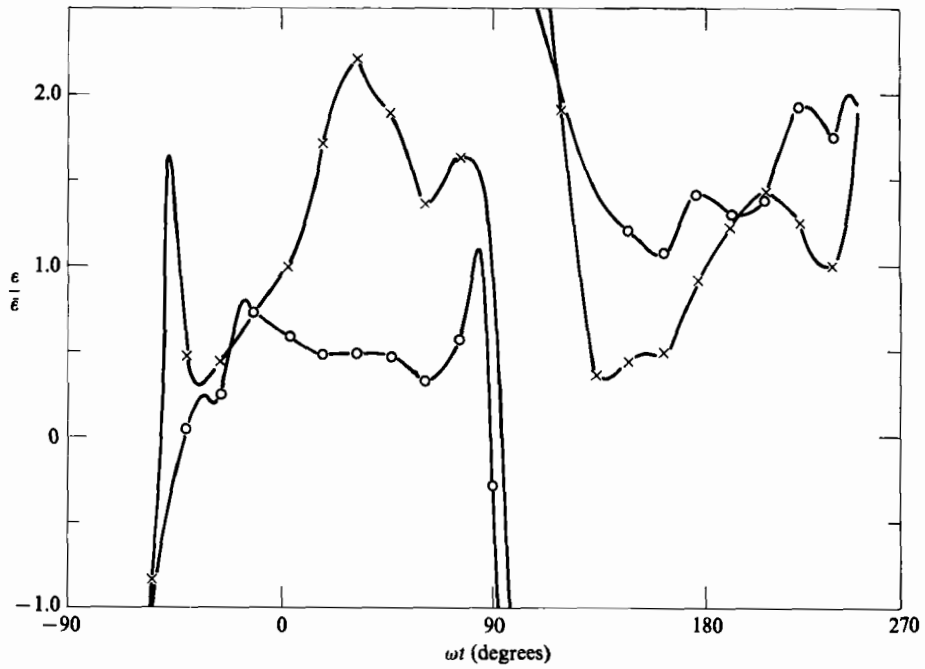

FIGURE 19. Variation of eddy viscosity during the course of the cycle: ×—×, $y = 3.5$ mm; ○—○, 30 mm: Test no. 4.

of the cycle varies with distance from the bed. For example, Kajiura (1968) assumed that for rough beds

$$\bar{\epsilon} = \text{const}, \quad \text{for } y < \tfrac{1}{2}k_s,$$

$$\bar{\epsilon} = K\hat{u}_* y, \quad \text{for } \tfrac{1}{2}k_s < y < 0.05\hat{u}_*/\omega,$$

$$\bar{\epsilon} = \text{const}, \quad \text{for } y > 0.05\hat{u}_*/\omega.$$

Figure 20 shows that there is indeed an intermediate range of heights for which $\bar{\epsilon} \propto \hat{u}_* y$. Similar curves were obtained for the other beds. However, for the present measurements the constant of proportionality is significantly different from usually accepted values for the Kármán constant K:

$$\text{For } D = 1.63 \text{ mm}, \quad K = 0.059,$$

$$D = 8.12 \text{ mm}, \quad K = 0.078,$$

$$D = 30.0 \text{ mm}, \quad K = 0.078.$$

These values of K could be increased to some extent if we were to argue that it is the mean value of u_* during the course of the half-cycle rather than its amplitude that influences the mean eddy viscosity. Measured ratios of $\hat{u}_*$ to $\overline{u}_*$ are given in table 1. If we equate $\bar{\epsilon}$ to $K\overline{u}_* y$ rather than to $K\hat{u}_* y$ the values of K become

$$\text{For } D = 1.63 \text{ mm}, \quad K = 0.10,$$

$$D = 8.12 \text{ mm}, \quad K = 0.11,$$

$$D = 30.0 \text{ mm}, \quad K = 0.13.$$

These values of K are still significantly less than the usually quoted figure of 0.4.

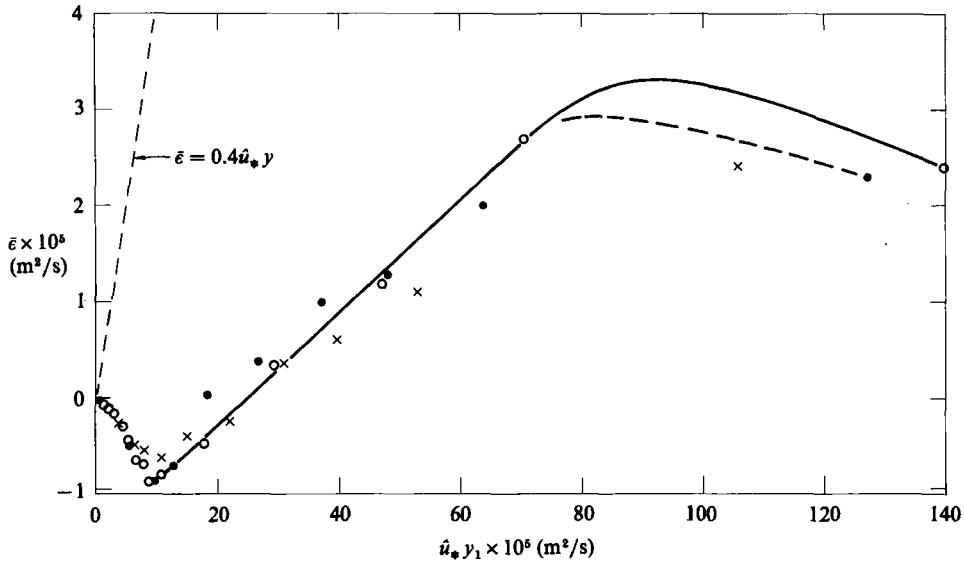

FIGURE 20. Variation of time-mean eddy viscosity with height: $D = 1.63$ mm. ○, Test no. 3; ●, Test no. 4; ×, Test no. 5.

The near-bed variation in $\bar{\epsilon}$ with height is also quite different from that usually assumed. For the 1.63 mm sand, $\bar{\epsilon}$ goes firmly negative near the bed and a similar, though less pronounced, trend was observed in the results for the 8.12 mm gravel. We note, in passing, that Jonsson & Carlsen (1976) found negative values of $\bar{\epsilon}$ very close to the bed in their Test no. 2 and that Hunt & Maxey (1978) showed, theoretically, that negative eddy viscosity might occur under certain circumstances. In figure 20 the zero for y_1 has been taken $0.35D$ below the mean level of the grain crests as suggested by Einstein (1950), to facilitate comparison with the results of other investigators. Although the choice of origin made little difference to the overall experimental scatter of the plots in terms of y/δ discussed above, it does make a significant difference for plots in terms of $\hat{u}_* y$.

Figure 21 shows the non-dimensionalized value of y_1 for which $\bar{\epsilon}$ passes through zero, i.e. the thickness of the inner layer in which $\bar{\epsilon}$ is negative. We see that the value of $\hat{u}_* y_1/\nu$ ranges from about 180 for the 1.63 mm sand up to about 280 for the 30.0 mm pebbles. These values of $\hat{u}_* y_1/\nu$ are far greater than normally accepted values for the thickness of the viscous sublayer in steady flow. This suggests that, whatever else is responsible for the unusual behaviour of $\bar{\epsilon}$, it is not simply a viscous-sublayer effect. We note also that the thickness is quite different from the value $\frac{1}{2}k_s$ suggested by Kajiura for the inner layer. For example, for Test no. 3 the measured thickness is about 10 mm whereas $\frac{1}{2}k_s$ is 1.63 mm. Figure 21 also shows that the value of $U_0 y_1/\nu$ is more or less constant at about 5200 for the range of a/k_s tested.

Making use of the data given in table 1 and making allowance for the different origins for y, we see that the region near the wall in which $\bar{\epsilon}$ is negative corresponds closely to the region in figure 14 in which the phase of maximum Reynolds stress is close to 0°. Further out, the maximum Reynolds stress shows a 180° phase change and $\bar{\epsilon}$ becomes positive. A possible explanation for these effects, based on the way in which fluid is thrown up when the vortices behind bed roughness elements are ejected at the end of each half-cycle, is put forward in §10.

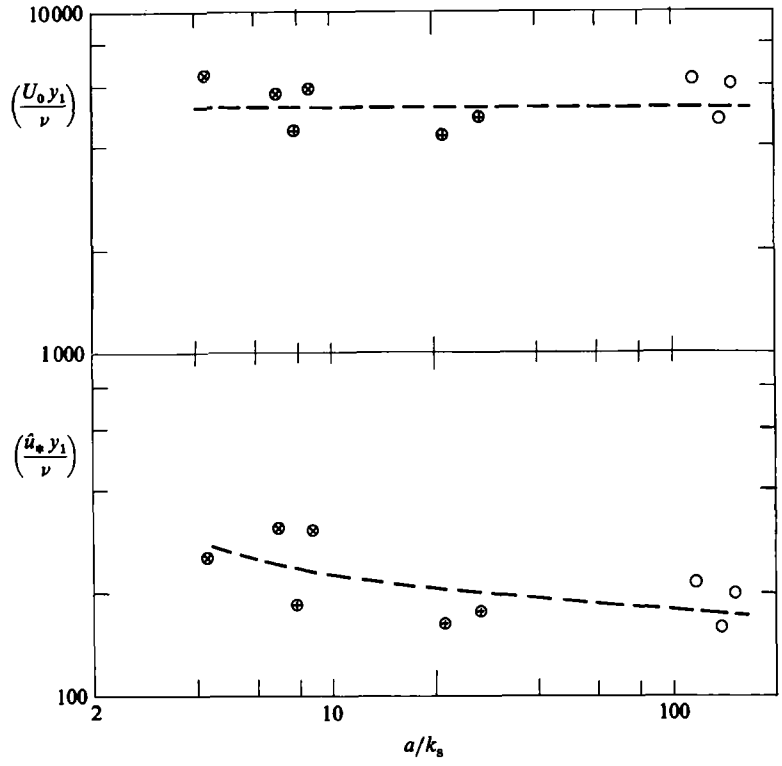

FIGURE 21. The height y_1 of the inner layer in which time-mean eddy viscosity is negative: ⊗, $D = 30.0$ mm; ⊕, 8.12 mm; ○, 1.63 mm.

At large distances from the bed figure 20 shows that $\bar{\epsilon}$ appears to decrease rather than remain constant as usually assumed. The constant value suggested by Kajiura (1968) in the outer layer is

$$\bar{\epsilon} = \frac{0.05 K \hat{u}_*^2}{\omega}, \tag{8}$$

whereas Brevik (1981) suggests

$$\bar{\epsilon} = \tfrac{1}{2} K \hat{u}_* \delta_1. \tag{9}$$

If we take $\hat{u}_*^2 = \frac{1}{2} U_0^2 f_w$ in these equations, with f_w given by Kajiura's (1968) theoretical curve, we see that both equations may be expressed in the form

$$\frac{\bar{\epsilon}\omega}{U_0^2} = f\left(\frac{a}{k_s}\right), \tag{10}$$

because the expression given by Jonsson (1980) for his boundary-layer thickness δ_1 is of the form

$$\frac{\delta_1}{k_s} = f\left(\frac{a}{k_s}\right). \tag{11}$$

Figure 22 shows the maximum value of $\bar{\epsilon}$ obtained from the results for the various rough beds compared with the curves suggested by Brevik and Kajiura. Clearly, the measured values of $\bar{\epsilon}$ in the outer layer are significantly less than the suggested values. Better agreement would have been obtained if we had calculated $\hat{u}_*$ in (8) and (9) from the experimental values based on Reynolds stress rather than Kajiura's (1968)

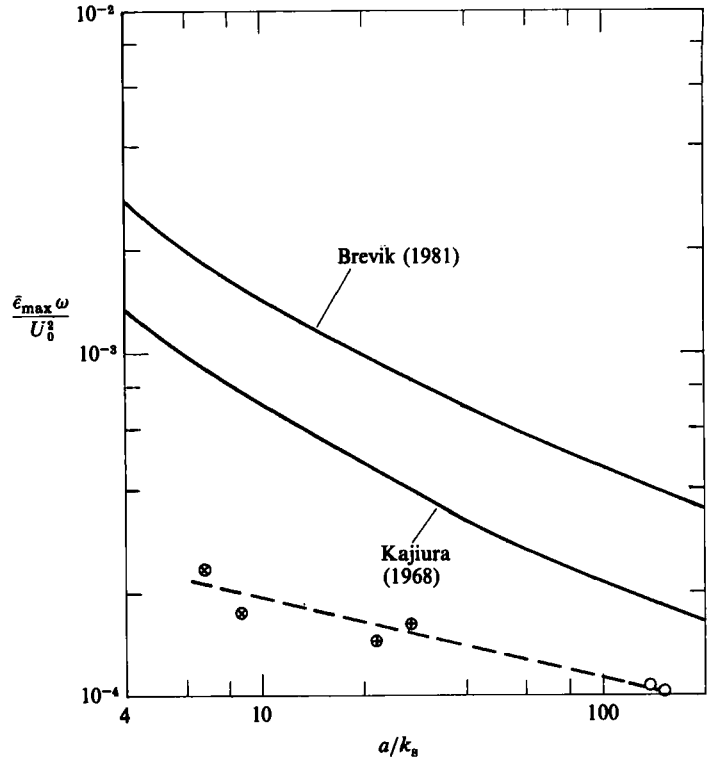

FIGURE 22. Variation with a/k_s of the maximum value of time-mean eddy viscosity. Symbols as for figure 21.

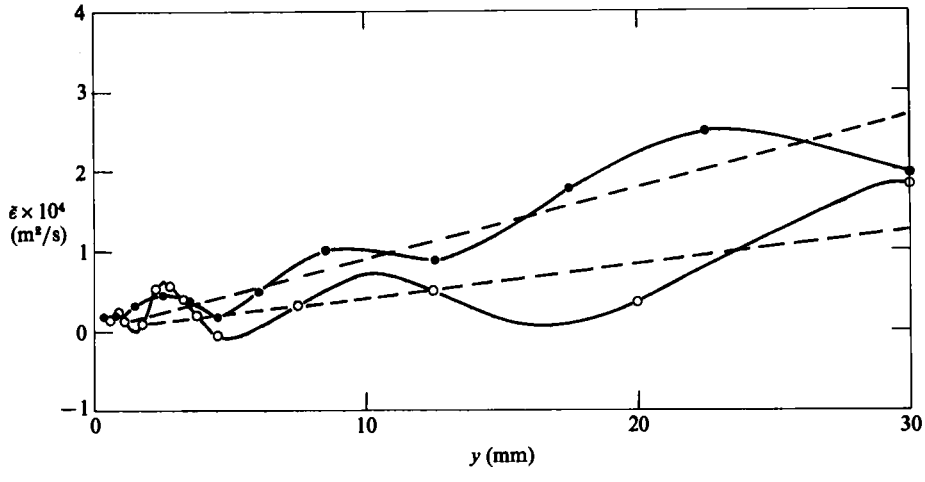

FIGURE 23. Variation with height of the time-mean eddy viscosity calculated with shear stress given by (5): ○, Test no. 3; ●, Test no. 4: $D = 1.63$ mm.

curve. However, the agreement would still not have been close, with Brevik's curve lying above the measurements and Kajiura's below.

So far, our comparisons have been based on the value of eddy viscosity obtained from (7) with τ equal to the Reynolds stress. Figure 23 shows how the mean eddy viscosity, averaged over the cycle, varies with height when τ is obtained from (5).

The general trend is for $\bar{\epsilon}$ to increase with y but with significant fluctuations about the mean. These fluctuations were larger for the rougher beds. Similar fluctuations in shear stress obtained from (5) were found by Jonsson & Carlsen (1976), who attributed them to slight inaccuracies in the measurement of free-stream velocity. However, even if we consider only the mean trend, the value of K in the relation $\bar{\epsilon} = K\hat{u}_* y$ is very different from the usually accepted values. For the results shown in figure 23 the dashed lines correspond to $K = 0.069$, for Test no. 3, $K = 0.16$, for Test no. 4, if $\hat{u}_*$ is based on the shear stress given by (5).

8. Mixing length

Some oscillatory-flow models make use of mixing-length arguments. For example, Bakker (1974) adopted the well-known relation

$$\tau = \rho l^2 \frac{\partial u}{\partial y}\left|\frac{\partial u}{\partial y}\right|, \tag{12}$$

with the mixing length

$$l = Ky. \tag{13}$$

Equation (12) may be written

$$l = u_*\Big/\frac{\partial u}{\partial y}. \tag{14}$$

Figure 24 shows an example of how the right-hand side of this equation varies during the course of the cycle for two different heights above the bed of 1.63 mm sand. Comparing with figure 19, which is for the same test conditions, we see that the mixing length varies during the course of the cycle in much the same way as the eddy viscosity. In particular, the mixing length also becomes infinite as the velocity gradient passes through zero.

Figure 25 shows how the mean value of the mixing length, defined by (14), varies with height for the bed of 1.63 mm sand. The test conditions are the same as for figure 20. In figure 25 the origin of y is the mean level of the grain crests. Since y is plotted directly there would be no change in the experimental scatter if the origin were taken $0.35D$ below the crest level as in figure 20. Once again, the mixing length shows similar trends to the eddy viscosity. For the 1.63 mm sand the mixing length initially becomes negative and then rises steadily. For the other beds the initial fall in mixing length with height is less marked but the trend is similar.

The conclusions to be drawn from figure 25 are also similar to those for the eddy viscosity. The initial negative region is too large to be explained away as a viscous sublayer. Presumably, its explanation is the same as that for the region of negative eddy viscosity mentioned earlier. The subsequent linear increase in mixing length with height is in agreement with (13) but, once again, the measured values of K are lower than those normally found in steady flow: for $D = 1.63$ mm, $K = 0.14$; for $D = 30.0$ mm, $K = 0.17$.

9. Ensemble-averaged velocity distribution

Figures 26 and 27 show typical examples of the way in which the amplitude and phase of the mean horizontal component of velocity vary with distance from the bed. The word mean is used to indicate the average obtained by superimposing the 200 cycles sampled at each height.

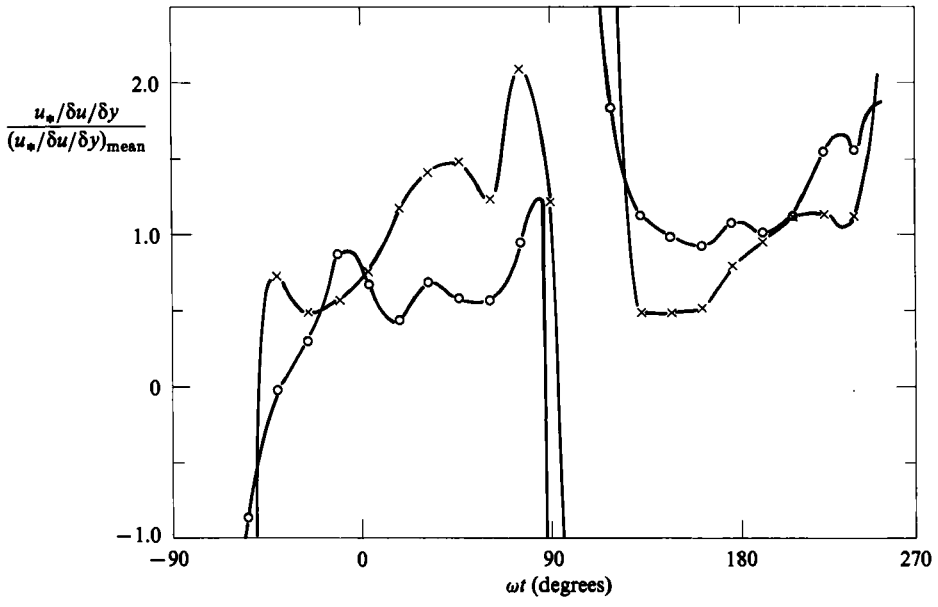

FIGURE 24. Variation of mixing length during the course of the cycle. Symbols as for figure 19.

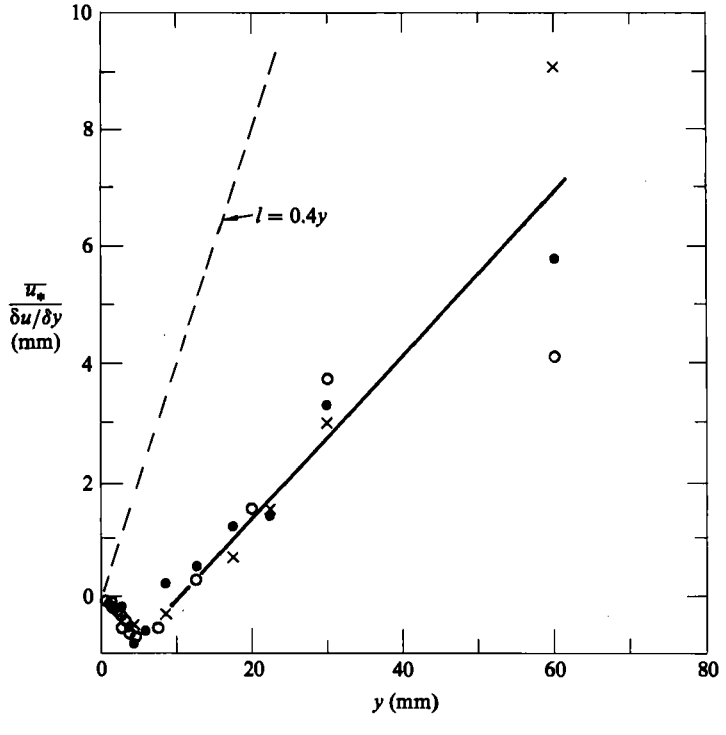

FIGURE 25. Variation of time-mean mixing length with height. Symbols as for figure 20.

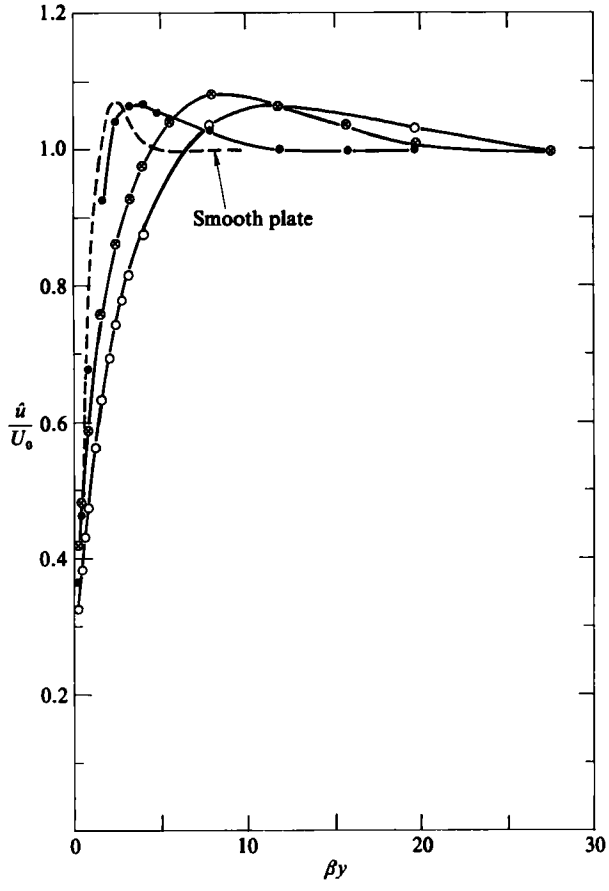

FIGURE 26. Variation with height of amplitude of ensemble-averaged horizontal component of velocity; $D = 1.63$ mm. ○, Test no. 3; ⊗, Test no. 5; ●, Test no. 7; ——, theoretical solution for flat plate.

The dashed curves represent the theoretical solution for laminar flow above an infinite flat plate (Lamb 1932). In addition to the rough-bed tests described here, tests have also been made with this anemometer with the bed composed of a sheet of glass. These show satisfactory agreement with the theoretical solution but are not reproduced in these figures in order to avoid confusion. Examples are, however, given in Du Toit & Sleath (1981).

The experimental profiles in figures 26 and 27 are similar to those obtained by other investigators. At low Reynolds numbers the profiles approximate to those for a flat plate but as the Reynolds number increases the boundary layer becomes progressively thicker. Although it is not very clear in figure 27, it was noticed that the phase measurements with this particular bed roughness showed a slight reduction in phase lead in the immediate vicinity of the bed. A similar trend was observed by Sleath (1970). It should be emphasized, however, that in the present case the measuring volume of the laser-Doppler anemometer is too large for any firm conclusion to be reached.

One of the more interesting studies of oscillatory-flow boundary layers is that of Jonsson (1980). In order to make a comparison with Jonsson's work we need to

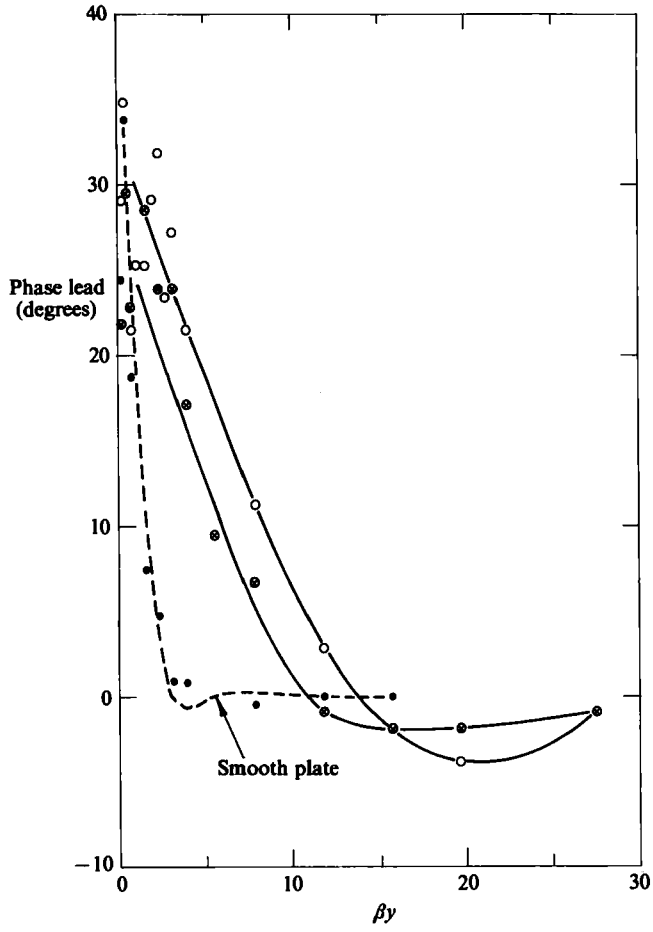

FIGURE 27. Phase variation with height of ensemble-averaged horizontal component of velocity. Symbols as for figure 26.

establish a link between the experimental values for the boundary-layer thickness used in this paper and the semi-empirical relation suggested by Jonsson:

$$\frac{30\delta_1}{k_s}\log\left(\frac{30\delta_1}{k_s}\right) = 1.20\frac{a}{k_s}. \tag{15}$$

Figure 28 shows that (15) gives significantly smaller values for the boundary-layer thickness than the measured values in table 1 but that the overall trend is similar to that of the experimental results. Figure 28 also includes values for the boundary-layer thickness, defined in the same way as for the present measurements, from the test results of Sleath (1982). It should be emphasized that Jonsson's definition of boundary-layer thickness is different from that used here. For laminar flow, the outer edge of his boundary layer corresponds to a defect velocity of amplitude $0.21U_0$. It is consequently not surprising that his curve should lie below the present measurements.

In general, we would expect δ/k_s to be a function of Reynolds number as well as a/k_s, as indicated by (1), except at very high values of $U_0 a/\nu$. The results in figure 28

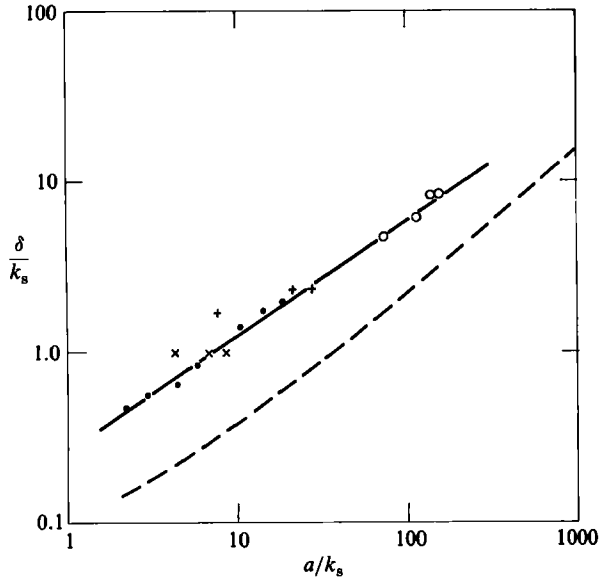

FIGURE 28. Variation of boundary-layer thickness with a/k_s. ×, $D = 30.0$ mm; +, 8.12 mm; ○, 1.63 mm; ●, tests of Sleath (1982); ---, (15).

do show some signs of Reynolds-number dependence for the tests with the two coarser beds.

It is interesting to examine whether the defect velocity outside the viscous sublayer is a function of y/δ alone, as found in steady flows, or whether it is also a function of a/k_s as suggested by (3). Figure 29 shows examples of the measured variation in defect velocity u_d with height. The results in figure 29(*b*) appear to show that it is not permissible to neglect a/k_s under the present conditions although the trends in figure 29(*a*), which shows the mean curves through the test results of Jonsson (1963) and Jonsson & Carlsen (1976), are less clear. The slight difference between these two curves may also be due to dependence on a/k_s. However, the discrepancy between these curves and the present results is more probably due to the different bed roughness in the two cases. In Jonsson's tests the roughness was two-dimensional.

In figure 29 the values of the boundary-layer thickness δ_1 and the shear velocity u_{1*} are those suggested by Jonsson (1980). The difference between the experimental results is somewhat reduced if the experimental values of δ and the shear velocity based on the measured Reynolds stress are used. However, there is still a slight, but apparently systematic, variation with a/k_s.

The results in figure 29 were plotted as $\log(y_1/\delta_1)$ versus $\hat{u}_d/\hat{u}_*$ in order to facilitate comparison with the measurements presented by Jonsson (1980). These axes make it difficult to follow the behaviour at large y_1/δ where (3) is most likely to be valid. Figure 30 shows $\log(\hat{u}_d/\hat{u}_*)$ plotted against y_1/δ for the results of Test no. 3 and also for the experimental results of Sleath (1982) with the largest Reynolds numbers. The agreement between the two sets of results is encouraging although there is a certain amount of experimental scatter. The straight line is drawn only as an indication of the general trend.

Sleath (1982) suggested that for large y the amplitude of the defect velocity could be expressed as

$$\hat{u}_d = \hat{u}_b \exp\left(\frac{-\beta y_1}{X}\right) \tag{16}$$

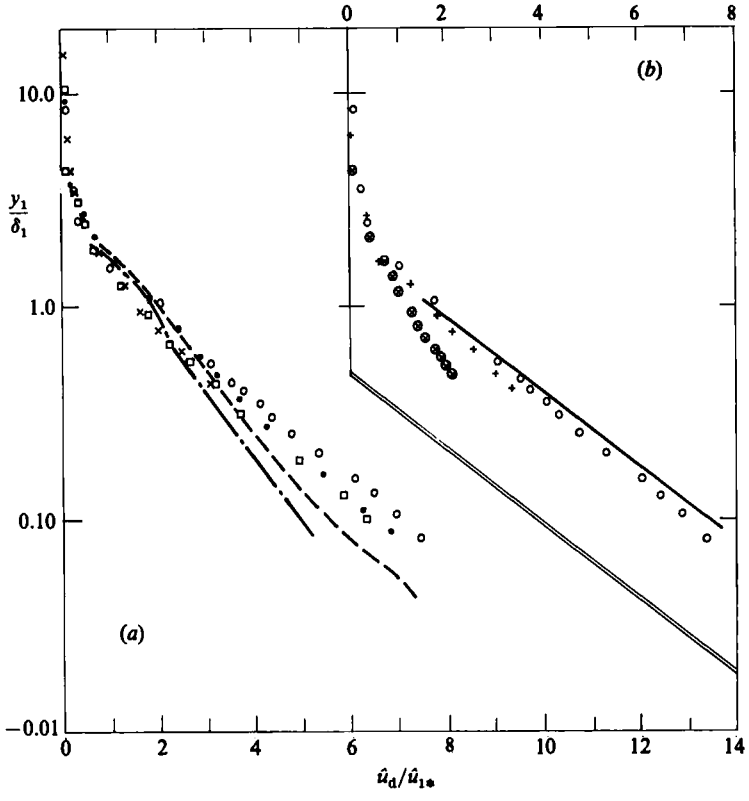

FIGURE 29. Variation of the amplitude of the ensemble-averaged defect velocity with height. (*a*) ○, Test no. 3; ●, Test no. 4; □, Test no. 5; ×, Test no. 6; ---, Jonsson (1963); —·—, Jonsson & Carlsen (1976). (*b*) ○, Test no. 3; +, Test no. 39; ⊗, Test no. 14; ——, (30).

where u_b is the value of the defect velocity at $y_1 = 0$, $\beta = (\omega/2\nu)^{\frac{1}{2}}$ and X is an empirical coefficient which is constant for any given set of test conditions. If it is true that

$$\frac{\hat{u}_d}{\hat{u}_*} = f\left(\frac{y_1}{\delta}\right), \tag{17}$$

it follows from comparison of (16) and (17) that

$$\frac{y_1}{\delta} \propto \frac{\beta y_1}{X}. \tag{18}$$

Jonsson (1980) suggested that a reasonable approximation to his expression for the boundary-layer thickness was

$$\frac{\delta_1}{k_s} = 0.072\left(\frac{a}{k_s}\right)^{\frac{3}{4}}. \tag{19}$$

Substituting in (18) gives

$$\frac{X}{(U_0 D/\nu)^{\frac{1}{2}}} \propto \left(\frac{a}{k_s}\right)^{\frac{1}{4}}, \tag{20}$$

if we assume $k_s \propto D$. On the other hand, the experimental results for boundary-layer thickness in figure 28 correspond to

$$\frac{\delta}{k_s} = 0.27\left(\frac{a}{k_s}\right)^{0.67}. \tag{21}$$

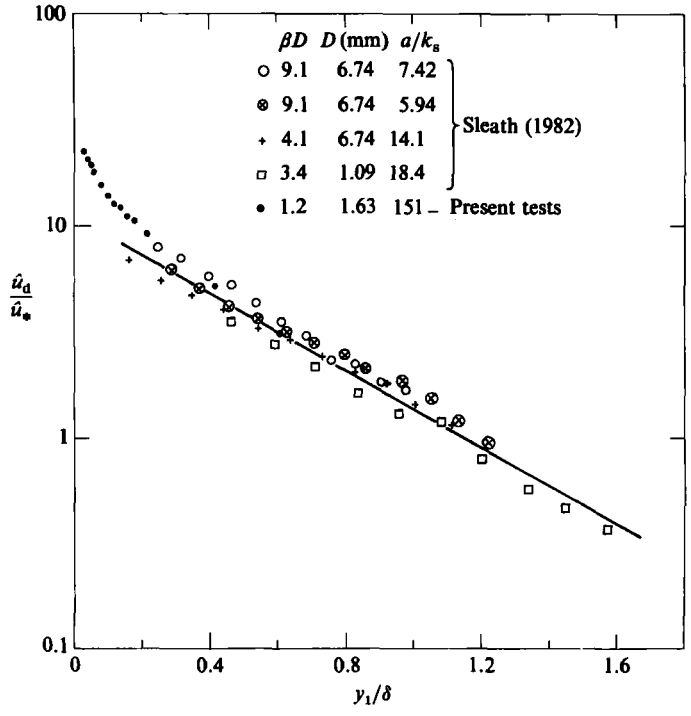

FIGURE 30. Comparison of results for Test no. 3 with results of Sleath (1982).

Substituting in (18) we obtain

$$\frac{X}{(U_0 D/\nu)^{\frac{1}{2}}} \propto \left(\frac{a}{k_s}\right)^{0.17}. \tag{22}$$

In fact, Sleath (1982) suggested that at large Reynolds numbers (as here)

$$\frac{X}{(U_0 D/\nu)^{\frac{1}{2}}} = 0.2. \tag{23}$$

Figure 31 shows that neither (20) nor (22) gives particularly good agreement with the experimental results of Sleath (1982) and Kalkanis (1964) for $U_0 D/\nu > 800$. In each equation the constant has been arbitrarily chosen to take the curve through the middle of the experimental points. Since Kalkanis' results cover only a rather limited range of y_1/δ it is possible that the values of X may have been systematically underestimated. It is also possible, however, that $\hat{u}_d/\hat{u}_*$ is a function of a/k_s as well as y_1/δ and that consequently neither (20) nor (22) is correct. It would only require a very small dependence of $\hat{u}_d/\hat{u}_*$ on a/k_s to bring (22) into agreement with the experimental results.

It may be noted that Nielsen (1985) suggested the empirical expression

$$\hat{u}_d \propto \exp\left(\frac{-y}{0.09(ak_s)^{\frac{1}{2}}}\right)^p, \tag{24}$$

where, for $a/k_s < 20$,

$$p \doteqdot 1. \tag{25}$$

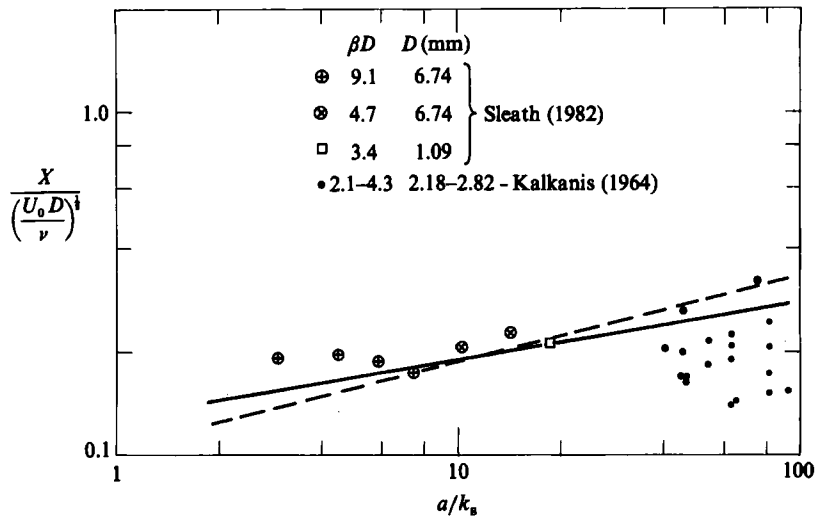

FIGURE 31. Variation of $X/(U_0 D/\nu)^{\frac{1}{2}}$ with a/k_s; ——, (22); – – –, (20).

Comparing the form of (24) and (16), as before, we obtain

$$\frac{X}{(U_0 D/\nu)^{\frac{1}{2}}} = 0.09\left(\frac{k_s}{2D}\right)^{\frac{1}{2}}. \tag{26}$$

If we assume $k_s \propto D$ we obtain

$$\frac{X}{(U_0 D/\nu)^{\frac{1}{2}}} = \text{const}, \tag{27}$$

which is of the same form as (23). However, to obtain exact agreement with (23) would require $k_s = 9.9D$ which is difficult to accept. The reason for the discrepancy is probably that Nielsen based his expression for Nikuradse roughness on measurements for two-dimensional bed roughness whereas the results in figure 31 are for three-dimensional roughness.

A somewhat similar result is obtained from examination of $\hat{u}_b$. Comparing (16) and (17) we have

$$\frac{\hat{u}_d}{\hat{u}_b} \propto \frac{\hat{u}_d}{\hat{u}_*}. \tag{28}$$

Thus

$$\frac{\hat{u}_b}{U_0} \propto \frac{\hat{u}_*}{U_0}. \tag{29}$$

Figure 32 shows the experimental results of Sleath (1982) and Kalkanis (1964) for which $U_0 D/\nu > 800$. Also shown are the curves for (29) obtained from Jonsson's (1963) expression for the friction factor and from the present experimental curve for friction factor based on Reynolds stress shown in figure 18. As before, the constant in each case has been arbitrarily chosen. The conclusion is the same as for figure 31: either the value of $\hat{u}_b$ in Kalkanis' tests has been systematically overestimated or $\hat{u}_d/\hat{u}_*$ is a function of a/k_s as well as y_1/δ.

Another question that has received considerable attention is whether oscillatory

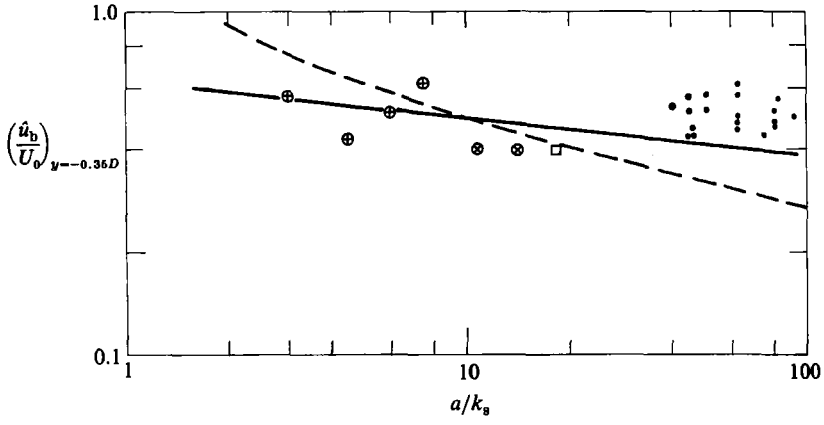

FIGURE 32. Variation of $\hat{u}_b/U_0$ with a/k_s. Symbols as for figure 31.

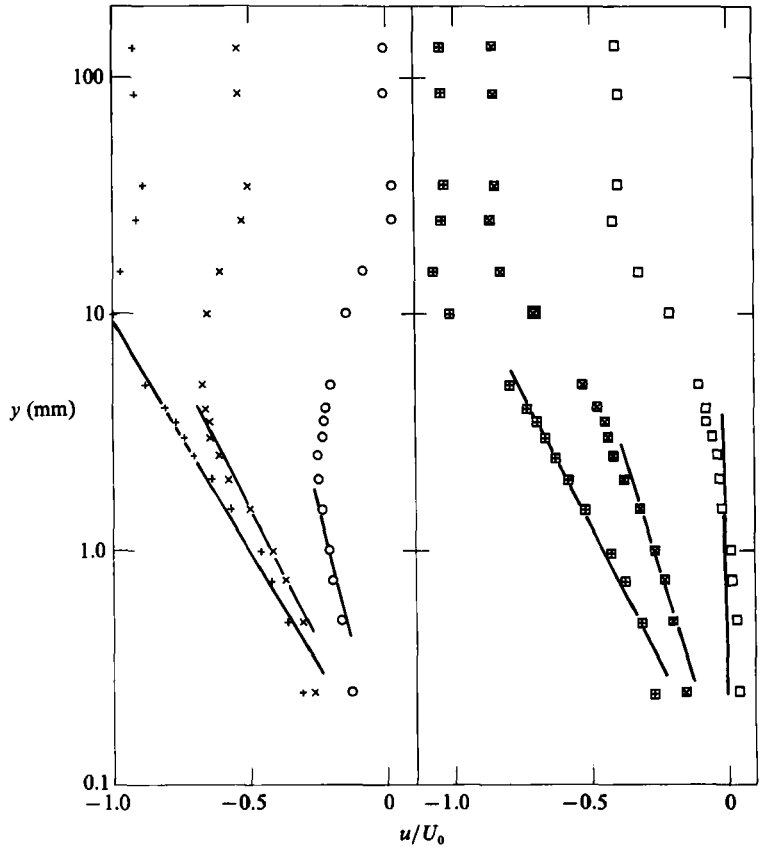

FIGURE 33. Examples of the fit of a semi-logarithmic curve to the experimental results for Test no. 3. Values of phase are: ○, −90°; ×, −60°; +, −30°; ⊞, 0°; ⊠, 30°; □, 60°.

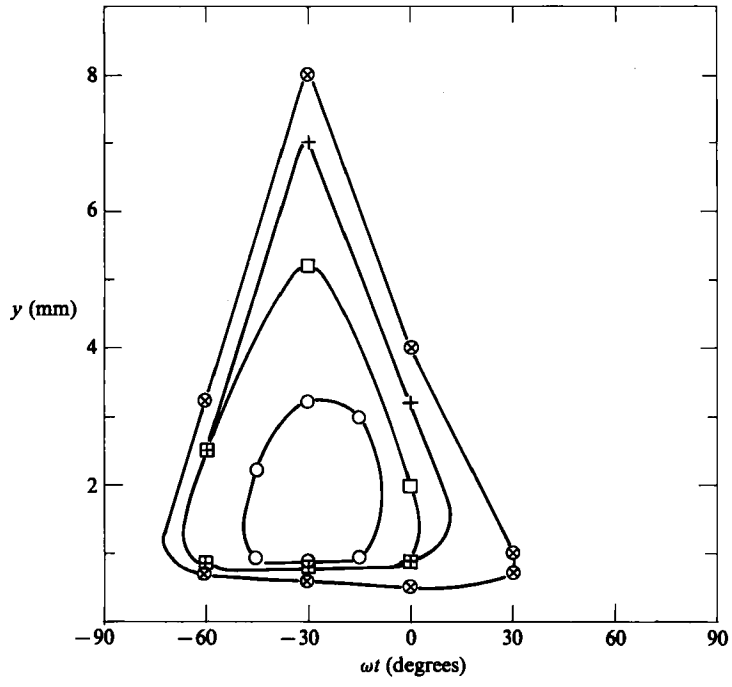

FIGURE 34. Range of values of y and ωt for which it is possible to fit a semi-logarithmic curve to the results for the ensemble-averaged horizontal velocity: $D = 1.63$ mm. ⊗, Test no. 3; +, Test no. 4; □, Test no. 5; ○, Test no. 6.

boundary layers have an 'overlap layer', and consequently a region of logarithmic velocity distribution, as in steady flow. The straight line in figure 29 (*b*) is of the form

$$\frac{\hat{u}_d}{\hat{u}_{1*}} = \frac{1}{0.4}\ln\left(\frac{y_1}{\delta_1}\right) + \text{const.} \tag{30}$$

We see that although the experimental points for Test no. 3 in figure 29 do follow a reasonable straight line over a wide range of y_1/δ_1 they do not quite follow (30). The results for other tests at lower values of a/k_s show even less good agreement. It is not surprising that Test no. 3 should show the closest agreement with the steady-flow curve since it has the largest value of a/k_s. If $\hat{u}_d/\hat{u}_{1*}$ does depend on a/k_s as well as y_1/δ_1 we would expect this a/k_s dependence to decrease as a/k_s becomes large.

Although the results for the amplitude of the defect velocity do not show close agreement with the logarithmic profile, it is possible to fit a logarithmic curve to the instantaneous velocity profiles, at least over a certain range of y and phase. This is illustrated in figure 33. The straight lines correspond to the expression suggested by Jonsson (1980):

$$\frac{u}{\hat{u}_{1*}} = -\frac{1}{0.4}\ln\left(\frac{30y}{k_s}\right)\cos(\omega t + \phi_0). \tag{31}$$

The angle ϕ_0 is the phase of $\hat{u}$ at $y = 0$, determined directly from the measurements, and $\hat{u}_{1*}$ is calculated from Jonsson's expression for the friction factor.

Figure 34 shows the range of y and phase for which it is possible to approximate the velocity distribution by (31) for the various tests with the 1.63 mm sand. As might

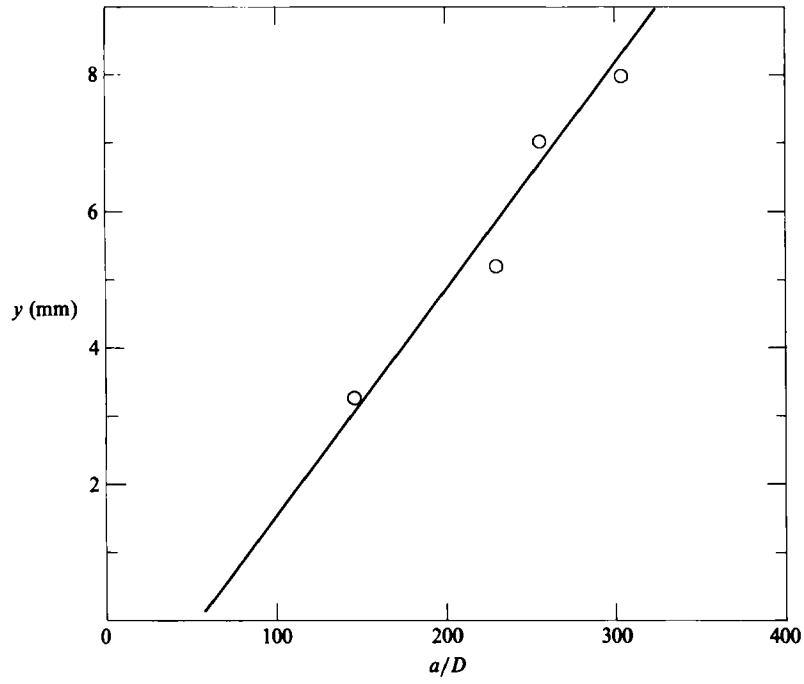

FIGURE 35. Variation with a/D of the range of y for which it is possible to fit a semi-logarithmic curve to the results for horizontal velocity: $D = 1.63$ mm.

be expected the range of y and phase over which it is possible to detect a logarithmic region in the velocity profile increases with increasing Reynolds number. This is illustrated by figure 35 which shows how the maximum height to which the logarithmic region extends increases with a/D. Extrapolation of these results back to the axis suggests that the logarithmic region might disappear altogether at $a/D \doteqdot 50$. This is reasonably close to the value of $a/k_s = 33$ suggested by Kajiura (1968) for the disappearance of the overlap layer. However, there are a number of reasons for treating this result with caution. First, Horikawa & Watanabe (1968) suggested that better agreement with Kajiura's results was shown by a limiting value $a/k_s = 115$. Secondly, we note in figure 34 that the greatest extent of the logarithmic region occurs before $\omega t = 0$ whereas figures 9 and 14 show maximum turbulence after $\omega t = 0$ for this range of y. Finally, it is clear from figure 33 that an equally good straight line might have been drawn through other segments of the velocity profile if the constants in (31) had been slightly different. This is, in fact, what was done by Hino *et al.* (1983) who concluded that the maximum extent of the logarithmic region occurred after $\omega t = 0$, as suggested by the turbulence intensities.

10. Jets and bursts

The measurements of Reynolds stress and eddy viscosity showed a number of surprising features. It is believed that the explanation for these effects is provided by the periodic formation of 'jets' or 'bursts' in the boundary layer. Several investigators have described how vortex formation and ejection in oscillatory flows over rough beds can cause fluid to be hurled away from the bed. This produced the

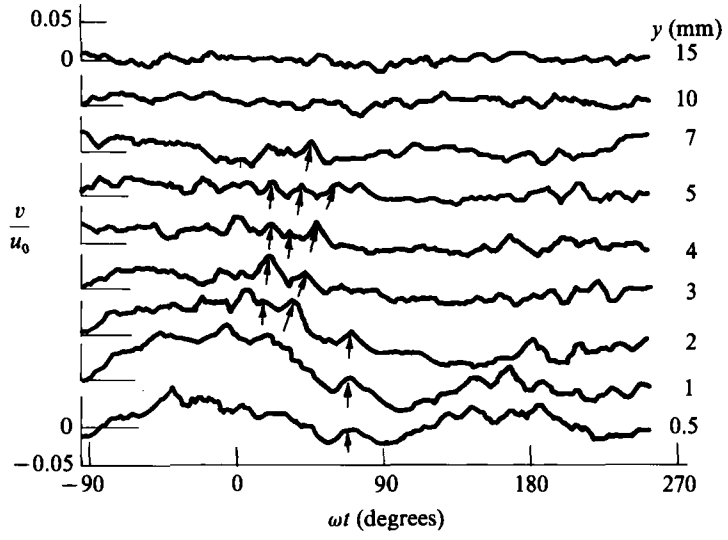

FIGURE 36. Variation with height and time of the ensemble-averaged vertical velocity: Test no. 4.

tongues of dye described by Vincent & Ruellan (1957) and Sleath (1970) and the surges in velocity measured by Keiller & Sleath (1976) and by George & Sleath (1978). In the laboratory these upward 'jets' of fluid seem to be most clearly defined for sands of median diameter about 1 or 2 mm. Coarser roughness produces more strongly formed vortices but also more chaotic exchanges of fluid from one layer to another.

Most observations of jets have been made with laminar flow. However, since they are caused by the ejection of vortices at the end of each half-cycle and since vortex formation by the bed roughness elements will continue even when the boundary layer is turbulent, jet formation is to be expected in turbulent flow too. In turbulent flow it is difficult to distinguish these 'jets' from the turbulent 'bursts' observed in steady flows except that they are associated with individual roughness elements on the bed and occur at a specific phase in the cycle.

Figure 36 shows vertical velocities at various heights for one of the tests with the 1.63 mm sand. Each record represents the average of 200 cycles and consequently turbulent fluctuations should have disappeared. If that is the case, the remaining fluctuations in vertical velocity must be due to a regular and repeatable effect such as the jet formation described above. The existence of multiple peaks in the record is presumably due to jets from several different roughness elements being convected through the measuring volume by the mean flow. Despite the fact that only a single-point measurement was made at each height, and consequently an upward jet at one height might not necessarily pass through the measuring volume at another, it is possible to follow some of the surges in velocity from one level to another as indicated by the arrows in figure 36. (The more general upsurges in velocity visible in figure 36 for y less than 3 mm are presumably due to local irregularities of the bed.)

The effect of these jets is to produce a net flux of momentum from one fluid layer to another. Figure 37 shows how the spatially averaged product of $\overline{u}$ and $\overline{v}$ varies during the course of the cycle in one of the tests with the 30.0 mm pebbles. The test conditions are the same as for figure 7 and the spatial average is the average of the measurements at the 29 different horizontal positions indicated in that figure. Even

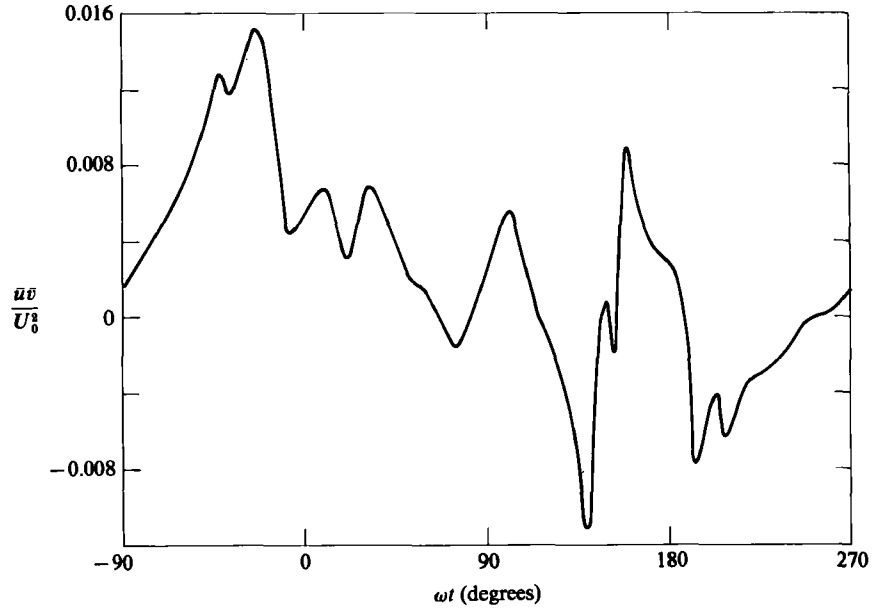

FIGURE 37. Variation during the course of the cycle of the spatially averaged value of $\overline{uv}$: Test no. 19; $y = 3$ mm.

this relatively large number of horizontal measuring points is probably insufficient to give an accurate average value for $\overline{u}\overline{v}$ but it is clear that there are indeed significant net momentum fluxes from one horizontal level to another. For purposes of comparison, it may be noted that the value of $\overline{u'v'}/U_0^2$, averaged over the same 29 horizontal positions, ranged from 0.0015 to −0.0014 in this test.

This upward flux of momentum provides a possible explanation for the discrepancy between values of f_w obtained from the Reynolds-stress measurements and those given by (5). The derivation of (5) assumes that the net flux of momentum (other than that due to turbulence) through any large horizontal plane is negligible at each instant in the cycle. Figure 37 shows that this is not so and that the magnitude of the neglected momentum flux is large enough to explain the discrepancy between the Reynolds stress and (5). Why then do the values of f_w calculated from (5) for the present test data agree with Kamphuis' (1975) direct measurements of bed shear? The reason is that when the lower boundary of the control volume used to derive (5) coincides with the surface of the bed there is no flux of momentum across it. Thus, (5) may be expected to give an accurate result for the horizontal force exerted by the fluid on the bed. However, for a rough bed this force is the sum of the shear stress exerted by the fluid and the integrated effect of the pressure gradient in the fluid acting over the surface of the bed roughness. The horizontal force due to the pressure gradient is far from negligible for rough beds and becomes very much larger than the fluid shear stress as $a/k_s \to 0$ (see e.g. Sleath 1984, p. 200). Thus, the agreement between (5) and Kamphuis' measurements of the horizontal force per unit area on the bed is not an indication that (5) gives an accurate result for the shear stress in the fluid. It might be argued that the quantity $\rho\overline{u}\overline{v}$ associated with the mean flux of momentum ought really to be incorporated into the Reynolds stress and that if this were done there would be no significant discrepancy between this 'Reynolds

stress' and the value for stress obtained from (5). The reason why this is unsatisfactory is that the quantity $\rho\bar{u}\bar{v}$ cannot be expected to vary with height and time in the same way as the Reynolds stress in a steady turbulent flow. Consequently, if this quantity were incorporated into the Reynolds stress the problem of modelling oscillatory flows would be even more complicated.

The existence of these jets of fluid also helps to explain the peculiar behaviour of the eddy viscosity near the bed. In effect, the flow near the bed is being driven by the fluid thrown up as the flow reverses. The Reynolds stress is a mere spectator in this process. There is, however, a link between the Reynolds stress and jet formation. Although the jets are associated with vortex ejection on flow reversal, and hence repeat themselves from cycle to cycle (as shown by the mean-velocity record in figure 36), they are not necessarily absolutely identical from one cycle to the next. The variations in jet velocity, direction and phase show up as increased values of $(\overline{u'^2})^{\frac{1}{2}}$, $(\overline{v'^2})^{\frac{1}{2}}$ and $\overline{u'v'}$. This explains why the maxima of $(\overline{u'^2})^{\frac{1}{2}}$, $(\overline{v'^2})^{\frac{1}{2}}$ and $\overline{u'v'}$ occur at more or less the same point in the cycle (figures 1, 2, 13) and why this is also the phase at which the fluctuations in the mean vertical velocity are most evident (figure 36).

The fact that, in the near-bed region, the jets are driving both the flow and the Reynolds stress explains why the mean eddy viscosity is negative. Further out, where the jets are no longer dominant, we would expect the Reynolds stress and eddy viscosity to return to the behaviour observed in steady flows. It is interesting to note in figure 36 that the vertical fluctuations in mean velocity disappear into the background noise at about $y = 10$ mm which is also, for this test, the height at which $\bar{\epsilon}$ once more becomes positive and the maximum Reynolds stress shows the 180° phase change. If the above model is correct, it is easy to understand why the thickness of the layer in which eddy viscosity is negative is much larger than that of a normal viscous sublayer.

Finally, it may be noted in passing that Sleath (1982) found that in the vicinity of the bed jets propagate up at more or less constant velocity. This would be consistent with the more or less constant upward velocity of propagation of the maxima of $(\overline{u'^2})^{\frac{1}{2}}$, $(\overline{v'^2})^{\frac{1}{2}}$ and $\overline{u'v'}$ in figures 9 and 14.

11. Conclusions

For the range of conditions covered in these experiments the main conclusions are as follows:

(i) Turbulence intensities fluctuate significantly during the course of the cycle. The variation has the approximate form of a modulated sine wave with two maxima per cycle. Close to the bed the turbulence reaches its maximum intensity as the flow decelerates. Further out, peak turbulence diffuses steadily out at an approximately constant velocity. In this outer region there is no obvious correlation between the phase of maximum turbulence intensity and any of the flow parameters.

(ii) Reynolds stress is significantly smaller than the shear stress evaluated using the usual momentum-integral approach. In particular, the maximum Reynolds stress is much less than the mean horizontal force per unit area on the bed. It is suggested that this discrepancy is due to the effect of the mean pressure gradient in oscillatory flows with rough beds and to the momentum transfers associated with vortex ejection on flow reversal.

(iii) Maximum Reynolds stress occurs at approximately the same phase as one of the maxima of turbulence intensity. However, as distance from the bed increases

another peak, in phase with the second maximum of turbulence intensity, begins to appear and eventually dominates the record.

(iv) Close to the bed the time-mean eddy viscosity at any given height is negative. This region correlates roughly with the region in which maximum Reynolds stress occurs at the first maximum of turbulence intensity rather than the second. It is suggested that these effects are also produced by the jets of fluid associated with vortex ejection on flow reversal. Further out, time-mean eddy viscosity increases steadily with height up to a maximum and then declines. In the region where eddy viscosity increases with height the rate of growth is slower than that usually found in steady flows.

(v) Variation of eddy viscosity during the course of the cycle is significant.

(vi) Variation of mixing length with time and with height is similar to that for eddy viscosity.

(vii) Mean-velocity profiles appear to show that, in the outer layer away from the bed, the non-dimensionalized defect velocity is a function of a/k_s as well as of y/δ.

REFERENCES

Bakker, W. T. 1974 Sand concentration in oscillatory flow. In *Proc. 14th Conf. on Coastal Engng, Copenhagen*, pp. 1129–1148. ASCE.

Bakker, W. T. & Van Doorn, T. 1978 Near bottom velocities in waves with a current. In *Proc. 16th Conf. on Coastal Engng, Hamburg*, pp. 1394–1413. ASCE.

Brevik, I. 1981 Oscillatory rough turbulent boundary layers. *J. Waterway Port Coastal Ocean Div. ASCE* **107** (WW3), 175–188.

Christoffersen, J. B. 1982 Current depth refraction of dissipative water waves. *Inst. Hydrodyn. Hydraul. Engng Tech. Univ. Denmark, Series paper* 30.

Corrsin, S. & Kistler, A. L. 1954 The free-stream boundaries of turbulent flows. *NACA Tech. Note* 3133.

Du Toit, C. G. & Sleath, J. F. A. 1981 Velocity measurements close to rippled beds in oscillatory flow. *J. Fluid Mech.* **112**, 71–96.

Einstein, H. A. 1950 The bed-load function for sediment transport in open channel flows. *U.S. Dept. of Agriculture. Soil Conservation Service. Tech. Bull.* 1026.

Fredsoe, J. 1981*a* Mean current velocity distribution in combined waves and current. *Inst. Hydrodyn. Hydraul. Res. Tech. Univ. Denmark Prog. Rep.* 53.

Fredsoe, J. 1981*b* A simple model for the wave boundary layer. *Inst. Hydrodyn. Hydraul. Res. Tech. Univ. Denmark Prog. Rep.* 54.

Fredsoe, J. 1982 Calculation of mean current profile in combined wave–current motion by application of the momentum equation. *Inst. Hydrodyn. Hydraul. Engng. Tech. Univ. Denmark Prog. Rep.* 55, 56.

George, C. B. & Sleath, J. F. A. 1978 Oscillatory laminar flow above a rough bed. In *Proc. 16th Conf. on Coastal Engng, Hamburg*, pp. 898–910. ASCE.

Grant, W. D. & Madsen, O. S. 1979 Combined wave and current interaction with a rough bottom. *J. Geophys. Res.* **84**, 1797–1808.

Hino, M., Kashiwayanagi, M., Nakayama, A. & Hara, T. 1983 Experiments on the turbulent statistics and the structure of a reciprocating oscillatory flow. *J. Fluid Mech.* **131**, 363–400.

Horikawa, K. & Watanabe, A. 1968 Laboratory study on oscillatory boundary layer flow. *Coastal Engng Japan* **11**, 13–28.

Hunt, J. C. R. & Maxey, M. R. 1978 Estimating velocities and shear stresses in turbulent flows of liquid metals driven by low frequency electromagnetic fields. In *MHD-Flows and Turbulence. II* (ed. H. Branover & A. Yakhot), pp. 249–269. Israel University Press.

Johns, B. 1975 The form of the velocity profile in a turbulent shear wave boundary layer. *J. Geophys. Res.* **80**, 5109–5012.

JOHNS, B. 1977 Residual flow and boundary shear stress in the turbulent bottom layer beneath waves. *J. Phys. Oceanogr.* **7**, 733–738.

JONSSON, I. G. 1963 Measurements in the turbulent wave boundary layer. In *Proc. 10th Congress IAHR, London*, pp. 85–92.

JONSSON, I. G. 1980 A new approach to oscillatory rough turbulent boundary layers. *Ocean Engng* **7**, 109–152.

JONSSON, I. G. & CARLSEN, N. A. 1976 Experimental and theoretical investigations in an oscillatory turbulent boundary layer. *J. Hydraul. Res.* **14**, 45–60.

KAJIURA, K. 1968 A model of the bottom boundary layer in water waves. *Bull. Earthquake Res. Inst.* **46**, 75–123.

KALKANIS, G. 1957 Turbulent flow near an oscillating wall. *Beach Erosion Board Tech. Memo.* 97.

KALKANIS, G. 1964 Transportation of bed material due to wave action. *US Army CERC Tech. Memo.* 2.

KAMPHUIS, J. W. 1975 Friction factors under oscillatory waves. *J. Waterway Harbors Coastal Eng. Div. ASCE* **101** (WW2), 135–144.

KEILLER, D. C. & SLEATH, J. F. A. 1976 Velocity measurements close to a rough plate oscillating in its own plane. *J. Fluid Mech.* **73**, 673–691.

KEMP, P. H. & SIMONS, R. R. 1982 The interaction between waves and a turbulent current: waves propagating with the current. *J. Fluid Mech.* **116**, 227–250.

KEMP, P. H. & SIMONS, R. R. 1983 The interaction between waves and a turbulent current: waves propagating against the current. *J. Fluid Mech.* **130**, 73–89.

KLEBANOFF, P. S. 1954 Characteristics of turbulence in a boundary layer with zero pressure gradient. *NACA Tech. Note* 3178.

LAMB, H. 1932 *Hydrodynamics*. Cambridge University Press.

LUNDGREN, H. 1972 Turbulent currents in the presence of waves. In *Proc. 13th Conf. on Coastal Engng, Vancouver*, pp. 623–634. ASCE.

NIELSEN, P. 1985 On the structure of oscillatory boundary layers. *Coastal Engng* **9**, 261–276.

SLEATH, J. F. A. 1970 Measurements close to the bed in a wave tank. *J. Fluid Mech.* **42**, 11–123.

SLEATH, J. F. A. 1982 The effect of jet formation on the velocity distribution in oscillatory flow over flat beds of sand or gravel. *Coastal Engng* **6**, 151–177.

SLEATH, J. F. A. 1984 *Sea Bed Mechanics*. Wiley Interscience.

SMITH, J. D. 1977 Modeling of sediment transport on continental shelves. In *The Sea*, vol. 6 (ed. E. D. Goldberg, I. N. McCave, J. J. O'Brien & J. H. Steele), pp. 539–577. Wiley Interscience.

TANAKA, H. & SHUTO, N. 1981 Friction coefficient for a wave–current coexistent system. *Coastal Engng Japan* **24**, 105–128.

VAN DOORN, T. 1981 Experimental investigation of near-bottom velocities in water waves without and with a current. *Delft Hydraulics Lab. Rep.* M1423 Part 1.

VINCENT, G. E. & RUELLAN, F. 1957 Mouvements solides provoqués par la houle sur un fond horizontal. *Houille Blanche*. B, 693–708.